Conformational Control of Intramolecular Electron Transfer in Calix[4]diquinones and Their Cationic Complexes

Anthony Harriman,*,† Muriel Hissler,† Pierre Jost,‡ Georges Wipff,*,‡ and Raymond Ziessel*,†

Contribution from the Laboratoire de Chimie, d'Electronique et Photonique Moléculaires, Ecole Européenne de Chimie, Polymères et Materiaux, and the Laboratoire de Modélisation et Simulations Moléculaires, Institut Le Bel, Université Louis Pasteur, 1 rue Blaise Pascal, F-67008 Strasbourg Cedex, France

Received August 4, 1998

Abstract: The synthesis is described of a photoactive molecular dyad comprising a luminescent ruthenium(II) tris(2,2′-bipyridyl) fragment covalently attached, via a methylene bridge, to a calix[4]arene receptor in which two of the four walls are benzoquinone functions. A distribution of interconverting conformers is expected for the calix[4]arene platform, including cone, partial cone, and 1,3-alternated forms, according to molecular dynamics simulations and NMR studies. Luminescence from the metal complex is quenched because of light-induced electron transfer from the triplet state to a nearby quinone. The MD simulations indicate that the redox-active subunits approach within orbital contact of each other and that the noncone conformations adopt coparallel arrangements of the redox partners that appear to be highly favorable for electron transfer. Cations, such as barium(II), are held at the lower rim of the receptor by coordination to the four O atoms and by two N atoms provided by an ancillary 2,2′-bipyridine that is appended to the receptor. Cation complexation increases slightly the thermodynamic driving force for light-induced electron transfer but restores luminescence from the ruthenium(II) tris(2,2′-bipyridyl) fragment. This apparent contradiction is explained in terms of the cation inducing a major structural modification of the supermolecule. Both MD and NMR studies indicate that the cation forces the luminophore away from the quinone and, by favoring the cone conformation of the calix-[4]arene, destabilizes cofacial orientations between closely spaced reactants. Consequently, the system functions as a sensitive photoionic detector.

Our understanding of electron-transfer processes has progressed enormously over the past 20 years or so, and especially in the past decade. Following a long hiatus during which the Marcus theory of outer-sphere electron transfer[1] was not universally accepted, there now exists a wealth of information regarding the many factors that combine to control the rate of an electron-transfer reaction in solution,[2] liquid−liquid junctions,[3] molecular complexes,[4] supramolecular arrays,[5] proteins,[6] and photosynthetic bacteria.[7] Without doubt, the two most important breakthroughs in this field were the implementation of molecular dyads[8−10] in which well-defined donor and acceptor groups were covalently linked into constrained structures having fixed geometry and the simultaneous development of ultrafast spectroscopic tools. Marcus theory,[1] with its numerous modifications and adaptations,[11] serves as the basis for interpreting kinetic data and for designing advanced synthetic systems. Although there are still important problem areas, particularly with ultrafast electron transfer between closely coupled reactants[12] and in special cases such as electron transfer in DNA,[13] attention is turning away from the fundamental issues and toward applications of electron transfer for analysis[14] and for construction of molecular-scale electronic devices.[15] Prominent among analytical protocols based on electron-transfer processes

† Laboratoire de Chimie, d'Electronique et Photonique Moléculaires.
‡ Laboratoire de Modélisation et Simulations Moléculaires.

(1) (a) Marcus, R. A. *J. Chem. Phys*. **1956**, *24*, 966. (b) Marcus, R. A. *Discuss. Faraday Soc*. **1960**, *29*, 21. (c) Marcus, R. A. *Annu. Phys. Chem*. **1964**, *15*, 155. (d) Marcus, R. A. *J. Chem. Phys.* **1965**, *43*, 679.

(2) (a) Hopfield, J. J. *Proc. Natl. Acad. Sci. U.S.A.* **1974**, *71*, 3640. (b) Jortner, J. *J. Chem. Phys*. **1976**, *64*, 4860. (c) Beratan, D. N.; Betts, J. N.; Onuchic, J. N. *Science* **1991**, *252*, 1285. (d) Bixon, M.; Jortner, J. *Chem. Phys*. **1993**, *176*, 467. (e) Swallen, S. F.; Weidemaier, K.; Tavernier, H. L.; Fayer, M. D. *J. Phys. Chem.* **1996**, *100*, 8106. (f) Barbara, P. F.; Meyer, T. J.; Ratner, M. A. *J. Phys. Chem*. **1996**, *100*, 13148. (g) Weidemaier, K.; Tavernier, H. L.; Swallen, S. F.; Fayer, M. D. *J. Phys. Chem. A* **1997**, *101*, 1887.

(3) (a) DeArmond, M. K.; DeArmond, A. H. In *Liquid−Liquid Interfaces*; Volkov, A. G., Deaner, D. W., Eds.; CRC: Boca Raton, 1996; p 255. (b) Dryfe, R. A. W.; Ding, Z.; Wellington, R. G.; Brevet, P. F.; Kurnetzov, A. M.; Girault, H. H. *J. Phys. Chem. A* **1997**, *101*, 2519.

(4) (a) Asahi, T.; Ohkohuchi, M.; Mataga, N. *J. Phys. Chem*. **1993**, *97*, 13132. (b) Gould, I. R.; Ege, D.; Moser, J. E.; Farid, S. *J. Am. Chem. Soc*. **1990**, *112*, 4290. (c) Gould, I. R.; Noukakis, D.; Gomez-Jahn, L.; Young, R. H.; Goodman, J. L.; Farid, S. *Chem. Phys.* **1993**, *176*, 439. (d) Brun, A. M.; Harriman, A.; Hubig, S. M. *J. Phys. Chem*. **1992**, *96*, 254. (e) Benniston, A. C.; Harriman, A.; Philp, D.; Stoddart; J. F. *J. Am. Chem. Soc*. **1993**, *115*, 5298. (f) Benniston, A. C.; Harriman, A. *J. Am. Chem. Soc*. **1994**, *116*, 11531. (g) Wynne, K.; Gali, C.; Hochstrasser, R. M. *J. Chem. Phys*., **1994**, *100*, 4797.

(5) (a) Harriman, A.; Kubo, Y.; Sessler, J. L. *J. Am. Chem. Soc*. **1992**, *114*, 388. (b) Sessler, J. L.; Wang, B.; Harriman, A. *J. Am. Chem. Soc*. **1993**, *115*, 10418. (c) Sessler, J. L.; Wang, B.; Harriman, A. *J. Am. Chem. Soc*. **1995**, *117*, 704. (d) Hayashi, T.; Miyahara, T.; Kumazaki, S.; Ogoshi, H.; Yoshihara, K. *Angew. Chem., Int. Ed. Engl*. **1996**, *35*, 1964. (e) Arimura, T.; Brown, C. T.; Springs, S. L.; Sessler, J. L. *Chem. Commun*. **1996**, 2293. (f) Kimura, M.; Misawa, Y.; Yamaguchi, Y.; Hanabusa, K.; Shirai, H. *Chem. Commun*. **1996**, 2785. (g) David, E.; Born, R.; Kaganer, E.; Joselevich, E.; Dürr, H.; Willner, I. *J. Am. Chem. Soc*. **1997**, *119*, 7778. (h) Roberts, J. A.; Kirby, J. P.; Wall, S. T.; Nocera, D. G. *Inorg. Chim. Acta* **1997**, *263*, 395. (i) Hunter, C. A.; Hyde, R. K. *Angew. Chem., Int. Ed. Engl*. **1996**, *35*, 1936. (j) McCafferty, D. G.; Friesen, D. A.; Danielson, E.; Wall, C. G.; Saderholm, M. J.; Erickson, B. W.; Meyer, T. J. *Proc. Natl. Acad. Sci. U.S.A.* **1996**, *93*, 8200. (k) Batchelder, T. L.; Fox, R. J.; Fox, M. A. *J. Org. Chem.* **1996**, *61*, 4206.

10.1021/ja982786v CCC: $18.00
Published on Web 12/22/1998

are luminescent sensors for which selective binding of cations at receptor sites modifies the luminescence yield of an adjacent chromophore by switching-on or -off intramolecular electron transfer.[14,16,17] Because the course of reaction is measured by luminescence spectroscopy, such sensors can be both simple and effective while electrogenerated chemiluminescence[18] provides for improved sensitivity. In several cases,[19] the mechanism by which cation complexation modulates the luminescence yield can be understood in terms of current electron-transfer theory.

A particularly straightforward, but elegant, example of a molecular dyad that displays luminescence on/off characteristics concerns the case of an emissive ruthenium(II) tris(2,2′-bipyridyl) complex appended by a short aliphatic chain to a benzoquinone moiety.[20] Fast intramolecular electron transfer occurs from the triplet excited state of the metal complex to the nearby quinone, followed by slower charge recombination, such that emission is extinguished. Electrochemical reduction of the quinone to the corresponding hydroquinol restores luminescence from the metal complex since the thermodynamic driving force for electron transfer is lost. This system is the prototype of a fast redox switch,[21] but since there is no suitable receptor site, it does not respond to the presence of adventitious cations. The latter facility can be realized most conveniently by building the quinone into a macrocyclic receptor that possesses the necessary functionality to complex certain cations from solution. A facile way to do this involves construction of a calix[4]diquinone in which two opposite walls of the macrocycle consist of benzoquinone units and the other two walls are provided by 4-*tert*-butylphenolic residues.[22] As for the above prototype, each quinone can be electrochemically reduced to the corresponding hydroquinol[23] while the calix[4]arene provides a functionalized cavity that might be expected to bind cations.[24] Appending one or more ruthenium(II) tris(2,2′-bipyridyl) fragment(s) is intended to provide a luminescent probe by which to monitor complexation, providing cation binding registers a change in luminescence yield and/or spectral profile. As such,

(6) (a) Onuchic, J. N.; Beratan, D. N.; Winkler, J. R.; Gray, H. B. *Annu. Rev. Biophys. Biomol. Struct*. **1992**, *21*, 349. (b) Moser, C. C.; Keske, J. M.; Warncke, K.; Farid, R. S.; Dutton, P. L. *Nature* **1992**, *355*, 796. (c) Beratan, D. N.; Onuchic, J. N.; Winkler, J. R.; Gray, H. B. *Science* **1992**, *258*, 1740. (d) Pelletier, H.; Kraut, J. *Science* **1992**, *258*, 1748. (e) Knapp, E. W.; Fischer, S. F. *J. Chem. Phys.* **1987**, *87*, 3880. (f) Pascher, T.; Chesick, J. P.; Winkler, J. R.; Gray, H. B. *Science* **1996**, *271*, 1558.

(7) (a) Parson, W. W. In *New Comprehensive Biochemistry: Photosynthesis*; Amesz, J., Ed.; Elsevier: Amsterdam, 1987; p 43. (b) Deisenhofer, J.; Michel, H. *Angew. Chem., Int. Ed. Engl*. **1989**, *28*, 829. (c) Huber, R. *Angew. Chem., Int. Ed. Engl*. **1989**, *28*, 848. (d) Plato, M.; Möbius, K.; Michel-Beyerle, M. E.; Bixon, M.; Jortner, J. *J. Am. Chem. Soc*. **1988**, *110*, 7279. (e) Fleming, G. R.; Martin, J. L.; Breton, J. *Nature* **1988**, *333*, 190. (f) Franzen, S.; Goldstein, R. F.; Boxer, S. G. *J. Phys. Chem*. **1993**, *97*, 3040. (g) Heller, B. A.; Holten, D.; Kirmaier, C. *Science* **1995**, *269*, 940. (h) Arnaut, L. G.; Formosinho, S. J. *J. Photochem. Photobiol., A* **1997**, *111*, 111.

(8) (a) Miller, J. R.; Calcaterra, L. T.; Closs, G. L. *J. Am. Chem. Soc*. **1984**, *106*, 5057. (b) Closs, G. L.; Calcaterra, L. T.; Green, N. J.; Penfield, K. W.; Miller, J. R. *J. Phys. Chem*. **1986**, *90*, 3673. (c) Closs, G. L.; Johnson, M. D.; Miller, J. R.; Piotrowiak, P. *J. Am. Chem. Soc*. **1989**, *111*, 3751. (d) Liang, L.; Miller, J. R.; Closs, G. L. *J. Am. Chem. Soc*. **1990**, *112*, 5353.

(9) (a) Wasielewski, M. R.; Niemczyk, M. P.; Svec, W. A.; Pewitt, E. B. *J. Am. Chem. Soc*. **1985**, *107*, 1080. (b) Irvine, M. P.; Harrison, R. J.; Beddard, G. S.; Leighton, P.; Sanders, J. K. M. *Chem. Phys*. **1986**, *104*, 315. (c) Joran, A. R.; Leland, B. A.; Folker, P. M.; Zewail, A. H.; Hopfield, J. J.; Dervan, P. B. *Nature* **1987**, *327*, 508. (d) Oevering, H.; Paddon-Row: M. N.; Heppener, M.; Oliver, A. M.; Corsaris, E.; Verhoeven, J. W.; Hush, N. S. *J. Am. Chem. Soc*. **1987**, *109*, 3258. (e) Finckh, P.; Heitele, H.; Volk, M.; Michel-Beyerle, M. E. *J. Phys. Chem*. **1988**, *92*, 6584. (f) Mataga, N.; Asahi, T.; Kanda, Y.; Okada, T.; Kakitani, T. *Chem. Phys*. **1988**, *127*, 249. (g) Brun, A. M.; Harriman, A.; Heitz, V.; Sauvage, J.-P. *J. Am. Chem. Soc*. ***1991***, *113*, 8657. (h) Fraser, D. D.; Bolton, J. R. *J. Phys. Chem*. **1994**, *98*, 1626.

(10) (a) Connolly, J. S.; Bolton, J. R. In *Photoinduced Electron Transfer*; Fox, M. A., Chanon, M., Eds.; Elsevier: Amsterdam, 1988; Part D, p 303. (b) Gust, D.; Moore, T. A. *Science* **1989**, *244*, 35. (c) Maruyama, K.; Osuka, A. *Pure Appl. Chem*. **1990**, *62*, 1511. (d) Wasielewski, M. R. *Chem. Rev*. **1992**, *92*, 435. (e) Harriman, A.; Sauvage, J.-P. *Chem. Soc. Rev*. **1996**, 41.

(11) (a) Ulstrup, J.; Jortner, J. *J. Chem. Phys*. **1975**, *63*, 4358. (b) Rips, I.; Jortner, J. *J. Chem. Phys*. **1987**, *87*, 2090. (c) Jortner, J.; Bixon, N. *J. Chem. Phys*. **1988**, *88*, 167. (d) Sumi, H.; Marcus, R. A. *J. Chem. Phys*. **1986**, *84*, 4272. (e) Kakitani, T.; Mataga, N. *J. Phys. Chem*. **1987**, *91*, 6277. (f) Sutin, N. *Acc. Chem. Res*. **1982**, *15*, 275. (g) Formosinho, S. J.; Arnaut, L. G.; Fausto, R. *Prog. React. Kinet*. **1998**, *23*, 1.

(12) (a) Gould, I. R.; Young, R. H.; Mueller, L. J.; Albrecht, A. C.; Farid, S. *J. Am. Chem. Soc*. **1994**, *116*, 8188. (b) Bixon, M.; Jortner, J.; Cortes, J.; Heitele, H.; Michel-Beyerle, M. E. *J. Phys. Chem*. **1994**, *98*, 7289. (c) Bixon, M.; Jortner, J.; Verhoeven, J. W. *J. Am. Chem. Soc*. **1994**, *116*, 7349. (d) Tachiya, M.; Murata, S. *J. Am. Chem. Soc*. **1994**, *116*, 2434. (e) Miyasaka, H.; Kotani, S.; Mataga, N. *J. Phys. Chem*. **1995**, *99*, 5757.

(13) (a) Murphy, C. J.; Arkin, M. R.; Jenkins, Y.; Ghatlia, N. D.; Bossmann, S. H.; Turro, N. J.; Barton, J. K. *Science* **1993**, *262*, 1025. (b) Brun, A. M.; Harriman, A. *J. Am. Chem. Soc*. **1992**, *114*, 3656. (c) Meade, T. J.; Kayyem, J. F. *Angew. Chem., Int. Ed. Engl*. **1995**, *34*, 352. (d) Lincoln, P.; Tuite, E.; Nordén, B. *J. Am. Chem. Soc*. **1997**, *119*, 1454. (e) Priyadarshy, S.; Risser, S. M.; Beratan, D. N. *J. Phys. Chem*. **1996**, *100*, 17678. (f) Arkin, M. R.; Stemp, E. D. A.; Holmlin, R. E.; Barton, J. K.; Hormann, A.; Olson, E. J. C.; Barbara, P. F. *Science* **1996**, *273*, 475. (g) Brun, A. M.; Harriman, A. *J. Am. Chem. Soc*. **1994**, *116*, 10383. (h) Lewis, F. D.; Wa, T.; Zhang, Y.; Letsinger, R. L.; Greenfield, S. R.; Wasielewski, M. R. *Science* **1997**, *277*, 673. (i) Meggers, E.; Kusch, D.; Spichty, M.; Wille, U.; Giese, B. *Angew. Chem., Int. Ed. Engl*. **1998**, *37*, 460. (j) Fukai, K.; Tanaka, K. *Angew. Chem., Int. Ed. Engl*. **1998**, *37*, 158.

(14) (a) Czarnik, A. W. In *Fluorescent Chemosensors for Ion and Molecule Recognition*; Czarnik, A. W., Ed.; ACS Symposium Series 538; American Chemical Society: Washington, DC, 1992. (b) de Silva, A. P.; Gunaatne, H. Q. N.; Gunlaugsson, T.; Huxley, A. J. M.; McCoy, C. P.; Rademacher, J. T.; Rice, T. E. *Chem. Rev*. **1997**, *97*, 1515. (c) Beer, P. D. *Acc. Chem. Res*. **1998**, *31*, 71.

(15) (a) Benniston, A. C. *Chem. Soc. Rev*. **1996**, *25*, 427. (b) Gosztola, D.; Yamada, H.; Wasielewski, M. R. *J. Am. Chem. Soc*. **1995**, *117*, 2041. (c) Harriman, A.; Ziessel, R. *Chem. Commun*. **1996**, 1707. (d) Steinberg-Yfrach, G.; Liddell, P. A.; Hung, S.-C.; Moore, A. L.; Gust, D.; Moore, T. A. *Nature* **1997**, *385*, 239. (e) Steinberg-Yfrach, G.; Rigaud, J.-L.; Durantini, E. N.; Moore, A. L.; Gust, D.; Moore, T. A. *Nature* **1998**, *390*, 479. (f) Seiler, M.; Dürr, H. *Liebigs Ann*. **1995**, 407. (g) Benniston, A. C.; Harriman, A.; Dimitri, S. *Angew. Chem., Int. Ed. Engl*. **1997**, *36*, 2356.

(16) For recent examples see: (a) Gong, Z.; Zhang, Z. *Anal. Chim. Acta* **1996**, *325*, 201. (b) Czarnik, A. W. *Trends Org. Chem*. **1993**, *4*, 123. (c) Piguet, C. *Chimia* **1996**, *50*, 144. (d) da Silva, A. P.; Gunaratna, H. Q. N.; Gunnlaugsson, T.; Nieuwenhuizen, M. *Chem. Commun*. **1996**, 1967. (e) da Silva, A. P.; Gunaratna, H. Q. N.; Gunnlaugsson, T.; Lynch, P. L. *New J. Chem*. **1996**, *20*, 871. (f) da Silva, A. P.; Nimal, H. Q.; Gunaratna, H. Q. N.; Gunnlaugsson, T.; McCoy, C. P.; Maxwell, P. R. S.; Rademacher, J. T.; Rice, T. E. *Pure Appl. Chem*. **1996**, *68*, 1443. (g) Barigelletti, F.; Flamigni, L.; Guardigli, M.; Sauvage, J.-P.; Collin, J.-P.; Sour, A. *Chem. Commun*. **1996**, 1329. (h) Takashita, M.; Irie, M. *Tetrahedron Lett*. **1988**, *39*, 613. (i) Gareis, T.; Huber, C.; Wolfbeis, O. S.; Daub, J. *Chem. Commun*. **1997**, 1717. (j) Collins, G. E.; Choi, L.-S. *Chem. Commun*. **1997**, 1135.

(17) Corresponding systems that register complexation of neutral or anionic species are also well-known. For recent examples, see: (a) Wannabe, S.; Onogowa, O.; Komatsu, Y.; Yoshida, K. *J. Am. Chem. Soc*. **1998**, *120*, 229. (b) Yam, V. W.-W.; Kai, A. S.-F. *Chem. Commun*. **1998**, 109. (c) Patterson, S.; Smith, B. D.; Taylor, R. E. *Tetrahedron Lett*. **1997**, *38*, 6323.

(18) (a) Xie, Z.-H.; Zhang, F.; Pan, Y.-S. *Analyst* **1998**, *123*, 273. (b) Kollmannsberger, M.; Gareis, T.; Heinl, S.; Brue, J.; Daub, J. *Angew. Chem., Int. Ed. Engl*. **1997**, *36*, 1333.

(19) (a) Gubelmann, M.; Harriman, A.; Lehn, J.-M.; Sessler, J. L. *J. Phys. Chem*. **1990**, *94*, 308. (b) Hissler, M.; El-ghayoury, A.; Harriman, A.; Ziessel, R. *Angew. Chem., Int. Ed. Engl*. **1998**, *37*, 1717. (c) Mathevet, R.; Jenusauskas, G.; Lapouyade, R.; Letard, J.-F.; Rulliere, C. *AIP Conf. Proc*. **1996**, *364 (Fast Elementary Processes in Chemical and Biological Systems)*, 358. (d) Tung, C.-H.; Wu, L.-Z. *J. Chem. Soc., Faraday Trans*. **1996**, *92*, 1381. (e) Borisenko, V. N.; Petrov, N. Kh.; Gromov, S. P.; Alfinov, M. V. *Khim. Fiz*. **1997**, *16*, 71.

(20) Goulle, V.; Harriman, A.; Lehn, J.-M. *J. Chem. Soc., Chem. Commun*. **1993**, 1034.

(21) Lehn, J.-M. In *Supramolecular Chemistry*; VCH Publishers: Weinheim, 1995.

(22) Morita, Y.; Agawa, T.; Kai, Y.; Kanchisa, N.; Kasai, N.; Nomura, E.; Taniguchi, H. *Chem. Lett*., **1989**, 1349.

(23) Suga, K.; Fujihira, M.; Monta, Y.; Agawa, T. *J. Chem. Soc., Faraday Trans*. **1991**, *87*, 1575.

(24) (a) Gutsche, C. D. In *Calixarenes, Monographs in Supramolecular Chemistry*; Stoddart, J. F., Ed; The Royal Society of Chemistry: Cambridge, 1989; Vol. 1. (b) Vicens, J.; Böhmer, V. In *Calixarenes: A Versatile Class of Macrocyclic Compounds*; Kluwer Academic Press: Dordrecht, 1991.

the success of the sensor depends on the ability of the cation to modify either the energetics for electron transfer or the conformation of the superstructure. Examples of the former case, where the cation binds to the lone pair of an amino donor, are well established,[14] and herein we describe an example of the latter family of sensors. It is shown that fixing a cation at the receptor site is accompanied by a small increase in the thermodynamic driving force for light-induced electron transfer but by a dramatic enhancement in luminescence yield.

Such calix[4]diquinones are not rigid entities but persist in solution in a variety of interconverting conformers, and in particular, it cannot be assumed that the so-called *cone* conformation will predominate. It has been demonstrated by NMR spectroscopy that the quinoid units can rotate about the axis provided by the bridging methylene groups, giving rise to partial cone (paco) or 1,3-alternated (1,3-alt) conformations.[25] A further complication concerns the use of a flexible connecting chain to link together luminophore and quencher since this seems certain to introduce additional conformational heterogeneity,[26] especially with two pendant luminophores. The absence of a well-defined ground-state geometry, while not detracting from the overall performance of the photosystem, makes it difficult to resolve the electron-transfer pathway.[27] For this reason, the connecting chain has been kept short while NMR studies and molecular-dynamics simulations have been made in an effort to elucidate the degree of internal flexibility of the superstructure in solution. It turns out that cation complexation freezes conformational exchange by restricting rotation of the calix[4]diquinone walls[28] and by elongating the connecting chain. These studies clarify the nature of the binding site and provide the necessary rationale by which to explain the relationship between cation binding and luminescence yield.

Experimental Section

Materials. Reagents used for synthesis of new compounds, such as thallium(III) trifluoroacetate, trifluoroacetic acid, potassium hexafluorophosphate, and ethanol, were obtained from commercial sources and used without additional purification. Compounds **L$_1$**,[29] **L$_2$**,[30] [Ru(bpy)$_2$Cl$_2$]·2H$_2$O,[31] and [Ru(d_8-bpy)$_2$Cl$_2$]·2H$_2$O[32] were prepared according to literature procedures. Acetonitrile was spectroscopic grade while the perchlorate salts used for complexation studies were of the highest available purity.

Ru(H). A mixture of [Ru(bpy)$_2$Cl$_2$]·2H$_2$O (0.026 g, 0.05 mmol) and the ditopic ligand **L$_1$** (0.050 g, 0.05 mmol) in ethanol (10 mL) was stirred at 80 °C for 15 h. After cooling to room temperature, potassium hexafluorophosphate (0.030 g, 0.15 mmol) in water (5 mL) was added. Slow evaporation of the organic solvent resulted in the precipitation of a red solid. This crude precipitate was chromatographed on alumina with CH$_3$OH/CH$_2$Cl$_2$ (5/95 by volume) as eluant. The product was recrystallized from acetone/ether to give a red solid (0.050 g, 60%). R_f = 0.57 (3 vol % CH$_3$OH in CH$_2$Cl$_2$, alumina). ^{1}H NMR (CDCl$_3$) δ = 8.94 (s, 1H); 8.50−7.02 (m, 33H); 6.81 (s, 2H); 6.75 (s, 2H); 5.11 (s, 2H, bpy−C*H*$_2$−O); 5.01 (AB quartet, 2H, J_{AB} = 13.1 Hz, $\Delta\nu$ = 25.9 Hz, bpy−C*H*$_2$−O); 3.80 (AB quartet, 2H, J_{AB} = 12.5 Hz, $\Delta\nu$ = 168.3 Hz, Ar−C*H*$_2$−Ar); 3.74 (AB quartet, 2H, J_{AB} = 12.8 Hz, $\Delta\nu$ = 169.0 Hz, Ar−C*H*$_2$−Ar); 3.48 (AB quartet, 2H, J_{AB} = 13.7 Hz, $\Delta\nu$ = 123.1 Hz, Ar−C*H*$_2$−Ar); 3.47 (AB quartet, 2H, J_{AB} = 13.7 Hz, $\Delta\nu$ = 156.1 Hz, Ar−C*H*$_2$−Ar); 2.36 (s, 3H, C*H*$_3$−bpy); 2.18 (s, 3H, C*H*$_3$−bpy); 1.29 (s, 9H, *tert*-butyl); 1.27 (s, 9H, *tert*-butyl); 0.96 (s, 9H, *tert*-butyl); 0.93 (s, 9H, *tert*-butyl). ^{13}C−{^{1}H} NMR (CDCl$_3$) δ = 156.4; 156.3; 156.1; 156.0; 155.7; 153.5; 153.0; 151.9; 151.5; 151.3; 151.1; 150.5; 150.2; 150.1; 149.6; 149.2; 148.6; 147.9; 147.7; 142.1; 142.0; 139.1; 138.2; 137.9; 137.5; 137.4; 135.7; 134.2; 132.6; 132.3; 132.1; 131.6; 128.2; 127.9; 127.8; 127.3; 125.9; 125.2; 124.0; 123.6; 120.9; 120.6; 75.2 (bpy−C*H*$_2$−O); 73.7 (bpy−C*H*$_2$−O); 34.0 (Ar−C*H*$_2$−Ar); 33.9 (Ar−C*H*$_2$−Ar); 31.7 (C*H*$_3$−*tert*-butyl); 31.4 (C(CH$_3$)$_3$−*tert*-butyl); 30.9 (C*H*$_3$-*tert*-butyl); 18.5 (C*H*$_3$−bpy); 18.2 (C*H*$_3$−bpy). FAB$^+$ (*m*-NBA) m/z = 1571.6 [M − PF$_6$ + H]$^+$; 1553.5 [M − PF$_6$ − OH]; 1425.6 [M − 2PF$_6$]. FT-IR (KBr) ν/cm^{-1} = 3423 (s); 2961 (s); 1653 (m); 1603 (m); 1559 (m); 1466 (s); 1363 (m); 1192 (m); 1092 (m); 1048 (s); 841 (s); 762 (m). UV−vis (CH$_3$CN) λ_{max}/nm (ϵ/M^{-1} cm^{-1}) = 451 (13 600); 289 (105 200); 245 (140 500). Anal. Calcd for C$_{88}$H$_{91}$N$_8$O$_4$RuP$_2$F$_{12}$ (M_r = 1715.76): C = 61.60; H = 5.35; N = 6.53. Found: C = 61.43; H = 5.09; N = 6.43.

Ru(Q). Method 1. To a solution of thallium(III) trifluoroacetate (0.057 g, 0.100 mmol) in trifluoroacetic acid (1 mL) was added **Ru(H)** (0.03 g, 0.017 mmol). The orange-red solution was protected from room light and stirred at room temperature for 2 h. After neutralization with cold aqueous sodium carbonate, the product was extracted with dichloromethane. The organic layer was dried over magnesium sulfate, filtered, and evaporated to dryness under vacuum. This crude product was dissolved in acetone and treated with an aqueous solution (ca. 2 mL) of potassium hexafluorophosphate (0.013 g, 0.07 mmol). Slow evaporation of the organic solvent afforded an orange precipitate. Chromatography of the crude material on alumina with CH$_3$OH/CH$_2$Cl$_2$ = 5/95 (v/v) as eluant gave 0.013 g (45%) of the analytically pure **Ru(Q)**.

Method 2. This method employed a similar experimental procedure as used for preparation of **Ru(H).** Thus, a mixture of **L2** (0.020 g, 0.021 mmol) and [Ru(bpy)$_2$Cl$_2$]·2H$_2$O (0.017 g, 0.032 mmol) in ethanol (10 mL) was stirred at 80 °C for 15 h. The precipitate was chromatographed on alumina with CH$_3$OH/CH$_2$Cl$_2$ = 1/99 (v/v) as eluant to give a partially purified product. Further purification was made by chromatography on alumina with CH$_3$OH/CH$_2$Cl$_2$ = 2/98 (v/v) as eluant, affording the red-orange complex **Ru(Q)** (0.010 g, 28%).

R_f = 0.44 (CH$_3$OH/CH$_2$Cl$_2$ = 10/90, v/v, alumina). ^{1}H NMR (d_6-acetone) δ = 9.03 (s, 1H); 8.76−7.22 (m, 27H); 7.16−6.95 (8 lines, 4H); 6.60 (br s, 2H); 6.52 (s, 1H); 6.29 (s, 1H); 5.08 (s, 2H, bpy−C*H*$_2$−O); 5.02 (AB quartet, 2H, J_{AB} = 15.3 Hz, $\Delta\nu$ = 24.1 Hz, bpy−C*H*$_2$−O); 4.02−3.24 (m, 8H, Ar−C*H*$_2$−Ar); 2.39 (s, 3H, C*H*$_3$−bpy); 2.20 (s, 3H, C*H*$_3$−bpy); 1.17 (s, 9H, *tert*-butyl); 1.16 (s, 9H, *tert*-butyl). ES-MS (CH$_3$CN) m/z = 1487.6 [M − PF$_6$]$^+$; 671.1 [M − 2PF$_6$]$^{2+}$. FT-IR (KBr) ν/cm^{-1} = 2956 (m); 1654 (s); 1603 (m); 1465 (m); 1298 (m); 1196 (m); 841 (s); 763 (m). UV−vis (CH$_3$CN) λ_{max}/nm (ϵ/M^{-1} cm^{-1}) = 451 (14 400); 288 (116 500); 251 (81 800). Anal. Calcd for C$_{80}$H$_{72}$N$_8$O$_6$RuP$_2$F$_{12}$ (M_r = 1632.51): C = 58.86; H = 4.45; N = 6.86. Found: C = 58.70; H = 4.23; N = 6.75.

Ru$_2$(H). A solution of [Ru(bpy)$_2$Cl$_2$]·2H$_2$O (0.043 g, 0.08 mmol) and silver tetrafluoroborate (0.038 g, 0.19 mmol) in Ar-purged ethanol (10 mL) was stirred at 80 °C for 2 h. After cooling to room temperature, the red solution was filtered over cotton-wool and transferred quanti-

(25) Casnati, A.; Cornelli, E.; Fabbi, M.; Bocchi, V.; Mori, G.; Ugozzoli, F.; Manotti-Lanfredi, A. M.; Pochini, A.; Ungaro, R. *Recl. Trav. Chim. Pays-Bas* **1993**, *112*, 384.

(26) (a) Helaja, J.; Tauber, A. Y.; Kilpelainen, I.; Paavo, H. *Magn. Reson. Chem.* **1997**, *35*, 619. (b) Zhang, H.; Zhang, M.; Shen, T. *J. Photochem. Photobiol., A* **1997**, *103*, 63. (c) Zhang, S.-L.; Lang, M. J.; Goodman, S.; Durnell, C.; Fidlar, V.; Fleming, G. R.; Yang, N. C. *J. Am. Chem. Soc.* **1996**, *118*, 9042. (d) Burgdorff, C.; Loehmannroeben, H.-G.; Sander, T. *J. Chem. Soc., Faraday Trans.* **1996**, *92*, 3043. (e) Jaeger, W.; Schneider, S.; Verhoeven, J. W. *Chem. Phys. Lett.* **1997**, *270*, 50. (f) Zimmt, M. B. *Chimia* **1997**, *51*, 82.

(27) Under illumination, an electron is promoted from a d-orbital localized on the ruthenium(II) center to one of the coordinated 2,2′-bipyridyl ligands, and most likely, electron migration among the three coordinated bpy groups competes effectively with electron transfer to a quinone. The important issue is to distinguish among electron-transfer processes occurring via σ-bonds of the connecting spacer group, by way of an interspersed solvent molecule, or upon orbital contact between the redox-active reactants. Recent attention has focused on designing model systems that permit such distinctions to be made. For examples see: (a) Gosztola, D.; Wang, B.; Wasielewski, M. R. *Photochem. Photobiol., A* **1996**, *102*, 71. (b) Higashida, S.; Tsue, H.; Sugiura, K.-S.; Kaneda, T.; Sakata, Y.; Tanaka, Y.; Taniguchi, S.; Okada, T. *Bull. Chem. Soc. Jpn.* **1996**, *69*, 1329.

(28) Iwamoto, K.; Ikada, A.; Araki, K.; Harada, T.; Shinkai, S. *Tetrahedron* **1993**, *49*, 9937.

(29) Ulrich, G.; Ziessel, R. *Tetrahedron Lett.* **1994**, *35*, 6299.

(30) Cano-Yelo Bettega, H.; Moutet, J.-C.; Ulrich, G.; Ziessel, R. *J. Electroanal. Chem.* **1996**, *406*, 247.

(31) Sullivan, B. P.; Salman, D. J.; Meyer, T. J. *Inorg. Chem.* **1978**, *17*, 3334.

(32) Chirayil, S.; Thummel, R. P. *Inorg. Chem.* **1989**, *28*, 813.

tatively via cannula to an ethanol solution (5 mL) of ligand $\mathbf{L_1}$ (0.04 g, 0.041 mmol). The solution was heated at 80 °C for 40 h, during which time the color changed from red to orange, before the solvent was removed under vacuum. The crude product was purified by column chromatography on alumina with CH_3OH/CH_2Cl_2 = 5/95 (v/v) as eluant. Anion exchange was performed after dissolution of the complex in the minimum amount of acetone followed by addition of potassium hexafluorophosphate (0.029 g, 0.16 mmol) in water (5 mL). Slow evaporation of the organic solvent gave a red precipitate which was recrystallized from acetone/ether (0.051 g, 53%). R_f = 0.42 (CH_3OH/CH_2Cl_2, 5/95, v/v, alumina). ^{1}H NMR (CD_3CN) δ = 8.54−6.96 (m, 54H); 4.94 (AB quartet, 2H, J_{AB} = 12.8 Hz, $\Delta\nu$ = 28.4 Hz, bpy−C*H*$_2$−O); 4.82 (AB quartet, 2H, J_{AB} = 12.4 Hz, $\Delta\nu$ = 40.4 Hz, bpy−C*H*$_2$−O); 3.54 (AB quartet, 2H, J_{AB} = 12.7 Hz, $\Delta\nu$ = 109.4 Hz, Ar−C*H*$_2$−Ar); 3.33 (AB quartet, 2H, J_{AB} = 12.8 Hz, $\Delta\nu$ = 63.0 Hz, Ar−C*H2*−Ar); 3.11 (AB quartet, 2H, J_{AB} = 12.5 Hz, $\Delta\nu$ = 124.4 Hz, Ar−C*H*$_2$−Ar); 3.10 (AB quartet, 2H, J_{AB} = 12.7 Hz, $\Delta\nu$ = 128.6 Hz, Ar−C*H*$_2$−Ar); 2.21 (s, 6H, C*H*$_3$−bpy); 1.22 (s, 18H, *tert*-butyl); 1.11 (s, 18H, *tert*-butyl). ^{13}C−{^{1}H} NMR (CD_3CN) δ = 157.8; 154.4; 153.3; 152.5; 152.2; 149.7; 144.3; 140.1; 139.3; 138.6; 135.1; 134.6; 128.9; 128.3; 127.0; 126.1; 125.1; 124.8; 123.9; 74.8 (bpy−*C*H$_2$−O); 34.7 (Ar−*C*H$_2$−Ar); 34.4 (Ar−*C*H$_2$−Ar); 32.2 (*C*(CH$_3$)$_3$−*tert*-butyl); 31.5 (*C*H$_3$−*tert*-butyl); 31.2 (*C*H$_3$−*tert*-butyl); 18.4 (*C*H$_3$−bpy). FAB$^+$ (*m*-NBA) *m*/*z* = 2274.8 [M − PF_6 − H]$^+$; 2130.0 [M − 2PF_6]$^+$. FT-IR (KBr) ν/cm^{-1} = 3440 (m); 2950 (m); 1604 (m); 1466 (m); 1244 (m); 1123 (w); 840 (s); 762 (m); 557 (s). UV−vis (CH_3CN) λ_{max}/nm (ϵ/M^{-1} cm^{-1}) = 452 (37 400); 288 (204 500); 244 (83 900). Anal. Calcd for $C_{108}H_{108}N_{12}O_4Ru_2P_4F_{24}\cdot CH_3CN$ (M_r = 2420.14 + 41.05): C = 53.68; H = 4.43; N = 7.40. Found: C = 53.68; H = 4.48; N = 7.78.

Ru$_2$(Q). This compound was prepared as described above for **Ru(Q)**.

Method 1. A mixture of **Ru$_2$(H)** (0.015 g, 0.006 mmol) and thallium trifluoroacetate (0.040 g, 0.072 mmol) in trifluoroacetic acid (1 mL) was stirred at room temperature for 2 h. The crude material was chromatographed on alumina with CH_3OH/CH_2Cl_2 = 5/95 (v/v) as eluant to give 0.008 g (57%) of the analytically pure complex.

Method 2. A solution of $\mathbf{L_2}$ (0.050 g, 0.053 mmol) and [Ru(bpy)$_2$Cl$_2$]·2H$_2$O (0.059 g, 0.113 mmol) in ethanol (10 mL) was stirred at 80 °C for 15 h. The precipitate was first chromatographed on alumina using a mixture of CH_2Cl_2/CH_3OH with a gradient of methanol (1−5%) followed by a second chromatography on alumina with CH_3OH/CH_2Cl_2 = 2/98 (v/v) as eluant to give the red-orange complex **Ru$_2$(Q)** (0.062 g, 49%).

R_f = 0.56 (CH_3OH/CH_2Cl_2, 2/98, v/v, alumina). ^{1}H NMR (CH3CN) δ = 8.54−7.14 (m, 44H); 7.01−6.88 (m, 4H); 6.43−6.34 (m, 4H); 4.77−4.60 (m, 4H, bpy−C*H*$_2$−O); 3.64−2.87 (m, 8H, Ar−C*H*$_2$−Ar); 2.22 (s, 6H, C*H*$_3$−bpy); 1.12 (s, 18H, *tert*-butyl). FAB$^+$ (*m*-NBA) *m*/*e* = 2193.8 [M − PF_6 + 3H]$^+$; 2047.9 [M − 2PF_6 + 2H]; 1900.9 [M − 3PF_6]. FT-IR (KBr) ν/cm^{-1} = 2963 (m); 2919 (m); 1655 (m); 1466 (m); 1385 (m); 1244 (m); 1109 (m); 843 (s); 764 (m); 730 (m); 557 (s). UV−vis (CH_3CN) λ_{max}/nm (ϵ/M^{-1} cm^{-1}) = 445 (29 500); 282 (173 400); 248 (80,300). Anal. Calcd for $C_{100}H_{88}N_{12}O_6Ru_2P_4F_{24}$ (M_r = 2335.89): C = 51.42; H = 3.80; N = 7.20. Found: C = 51.43; H = 3.75; N = 7.52.

Samples of partially deuterated complexes were prepared using similar experimental conditions as described for the isolation of **Ru(Q)** (method 2). Ethanol (10 mL) containing [Ru(d_8-bpy)$_2$Cl$_2$]·2H$_2$O (0.100 g, 0.18 mmol) and the ditopic ligand $\mathbf{L_2}$ (0.080 g, 0.09 mmol) was heated at 80 °C for 24 h. After cooling to room temperature, potassium hexafluorophosphate (0.091 g, 0.49 mmol) in water (5 mL) was added. Slow evaporation of the organic solvent resulted in precipitation of a red solid. This crude precipitate contained both mono- and dinuclear complexes, which were separated by successive chromatography on alumina using CH_3OH/CH_2Cl_2 as eluant with a gradient of CH_3OH (0−10, v/v). The two compounds were further purified by recrystallization from acetone/ether.

Ru(Q)$_D$. Yield 0.053 g (37%). R_f = 0.43 (alumina, CH_3OH/CH_2Cl_2, 2/98, v/v). ^{1}H NMR (d_6-acetone) δ = 9.01 (br s, 1H); 8.64 (d, 1H, ^3J = 8.6 Hz); 8.50 (d, 1H, ^3J = 8.3 Hz); 8.49 (s, 1H); 8.42 (d, 1H, ^3J = 8.3 Hz); 8.33 (s, 1H); 8.29 (d, 1H, ^3J = 8.3 Hz); 8.21 (d, 1H, ^3J = 8.1 Hz); 7.99 (dd, 1H, ^3J = 8.1 Hz, ^4J = 2.2 Hz); 7.85 (s, 1H); 7.72 (d, 1H, ^3J = 8.3 Hz); 7.59 (dd, 1H, ^3J = 8.1 Hz, ^4J = 2.2 Hz); 7.12−7.00 (8 lines, 4H); 6.57 (m, 2H); 6.49 (br s, 1H); 6.25 (br s, 1H); 5.06 (s, 2H); 4.92 (AB quartet, 2H, J_{AB} = 13.2 Hz, $\Delta\nu$ = 25.6 Hz); 3.70 (AB quartet, 2H, J_{AB} = 11.7 Hz, $\Delta\nu$ = 105.0 Hz); 3.69 (AB quartet, 2H, J_{AB} = 13.0 Hz, $\Delta\nu$ = 96.3 Hz); 3.50 (AB quartet, 2H, J_{AB} = 14.0 Hz, $\Delta\nu$ = 65.2 Hz); 3.40 (AB quartet, 2H, J_{AB} =13.8 Hz, $\Delta\nu$ = 45.4 Hz); 2.37 (s, 3H); 2.19 (s, 3H); 1.16 (s, 18H); 1.14 (s, 18H). ^{13}C−{^{1}H} NMR (CD_3CN) δ = 188.0; 186.6; 186.4; 157.9; 157.6; 157.5; 157.2; 155.6; 154.9; 154.1; 152.8; 152.6; 150.6; 149.0; 148.9; 148.8; 148.7; 148.3; 139.6; 139.2; 138.3; 135.5; 134.7; 133.7; 133.1; 133.0; 132.9; 131.9; 131.5; 131.3; 128.4; 128.2; 128.0; 124.6; 124.4; 120.6; 71.8 (bpy−*C*H$_2$−O); 71.7 (bpy−*C*H$_2$−O); 33.5 (Ar−*C*H$_2$−Ar); 33.1 (Ar−*C*H$_2$−Ar); 33.0 (Ar−*C*H$_2$−Ar); 32.9 (Ar−*C*H$_2$−Ar); 31.5 (*C*H$_3$−*tert*-butyl); 30.2 (*C*(CH$_3$)$_3$); 18.4 (*C*H$_3$−bpy); 18.2 (*C*H$_3$−bpy). Anal. Calcd for $C_{80}H_{56}D_{16}N_8O_6RuP_2F_{12}\cdot CH_3CN\cdot C_7H_8$ (M_r = 1781.8 + 41.05 + 92.14): C = 59.99; H = 5.6; N = 7.07. Found: C = 60.19; H = 6.00; N = 7.12.

Ru$_2$(Q)$_D$. Yield 0.024 g (17%). R_f = 0.33 (alumina, CH_3OH/CH_2Cl_2, 2/98, v/v). ^{1}H NMR (d_6-acetone) δ = 8.67 (d, 2H, ^4J = 2.9 Hz); 8.63 (d, 2H, ^4J = 2.9 Hz); 8.16−8.06 (m, 4H); 7.99 (d, 2H, ^3J = 7.7 Hz); 7.88 (s, 2H); 7.02−6.88 (8 lines, 4H); 6.45 (s, 1H); 6.40 (br s, 1H); 6.26 (br s, 2H); 4.92−4.73 (2 AB quartet hidden, 4H); 3.78−3.02 (m, 8H); 2.81 (s, 6H); 1.05 (s, 18H). ^{13}C−{^{1}H} NMR (CD_3CN) δ = 189.3; 189.0; 188.7; 186.3; 158.1; 157.9; 157.8; 154.8; 152.8; 152.0; 148.9; 148.1; 148.0; 140.1; 139.5; 138.3; 137.7; 133.3; 130.9; 130.6; 128.5; 128.2; 127.9; 124.8; 124.3; 71.5 (bpy−*C*H$_2$−O); 33.8 (Ar−*C*H$_2$−Ar); 33.6 (Ar−*C*H$_2$−Ar); 33.3 (Ar−*C*H$_2$−Ar); 32.9 (Ar−*C*H$_2$−Ar); 31.6 (*C*H$_3$−*tert*-butyl); 30.1 (*C*(CH$_3$)$_3$); 18.6 (*C*H$_3$−bpy). Anal. Calcd for $C_{100}H_{56}D_{32}N_{12}O_6Ru_2P_4F_{24}\cdot CH_3CN\cdot C_7H_8$ (M_r = 2368.14 + 41.05 + 92.14): C = 52.32; H = 5.27; N = 7.28. Found: C = 52.58; H = 5.52; N = 7.62.

Methods. Nuclear magnetic resonance spectra were recorded at room temperature on Bruker SY-200 or AC-200 instruments at 200 MHz for ^{1}H NMR and 50 MHz for ^{13}C NMR. ^{1}H NMR chemical shifts (δ) are reported in parts per million (ppm) relative to residual protiated solvents (7.26 for $CDCl_3$, 2.04 for d_6-acetone, and 1.94 ppm for CD_3CN); ^{13}C−{^{1}H} NMR chemical shifts are reported relative to $CDCl_3$ (77.00 ppm), d_6-acetone (206.00, 29.80 ppm), and CD_3CN (181.21, 1.32 ppm). All carbon signals were detected as singlets. Fast-atom bombardment (FAB, positive mode) mass spectra were recorded on a ZAB-HF-VB analytical apparatus in a *m*-nitrobenzyl alcohol (*m*-NBA) matrix with Ar atoms being used for bombardment (8 keV). All relevant patterns had the expected isotopic profile, as confirmed by computer simulation. Electrospray mass spectra (ES-MS) were recorded on a Bio-Q analytical apparatus in acetone using grammicidim as internal standard. Routine absorption spectra were measured in CH_3CN at room temperature with a Kontron Uvikon 941 spectrophotometer. FT-IR spectra were recorded for KBr pellets or in solution with KBr cells using an IFS-25 Bruker spectrometer. Evidence for the assigned molecular formulas is based on ^{1}H and ^{13}C−{^{1}H} NMR spectra with selected homodecoupling experiments. Carbon assignments were made from appropriate DEPT experiments.

Absorption spectra were recorded with a Kontron Uvikon 930 spectrophotometer while luminescence spectra were recorded with a Perkin-Elmer LS50 spectrofluorimeter. All luminescence measurements were made with deoxygenated solutions, unless stated otherwise, using a stabilized, mode-locked argon ion laser operating at 514 nm as the excitation source. Luminescence quantum yield determinations were made by reference[33] to tris(2,2′-bipyridyl)ruthenium(II) in deoxygenated acetonitrile (Φ_L = 0.062). Triplet lifetimes were measured by time-resolved luminescence spectroscopy after laser excitation at 532 nm. For long-lived emission, excitation was made with a Q-switched, frequency-doubled Nd:YAG laser (fwhm = 4 ns) operated at 10 Hz. Luminescence was isolated from scattered laser light with a high-radiance monochromator and detected with a red-sensitive photomultiplier tube. The signal was transferred to a fast digitizer and stored on a microcomputer. The laser pulse was deconvoluted from the experimental record after averaging 256 individual records and analyzed by nonlinear least-squares iteration using the Levenberg−Marquardt

(33) Kober, E. M.; Marshall, J. L.; Dressick, W. J.; Sullivan, B. P.; Caspar, J. V.; Meyer, T. J. *Inorg. Chem.* **1985**, *24*, 2755.

algorithm. The time resolution of this instrument was ca.. 10 ns, being limited by the non-Gaussian shape of the laser pulse.

Improved temporal resolution was achieved using a mode-locked, frequency-doubled Nd:YAG laser (fwhm = 20 ps) as excitation source and with a fast response photodiode, cooled to 77 K, as detector. In this case the time resolution of ca. 100 ps was set by the rise time of the detector. Triplet lifetimes were also measured by transient absorption methodology following the recovery of ground-state chromophore at 450 nm. Solutions were deoxygenated before laser photolysis and were adjusted to possess an absorbance of ca. 0.25 at 532 nm. The same approach was used to monitor absorption spectral changes over the time range 25 ps to 10 ns. In all cases, the monitoring beam was provided with a white light continuum generated by focusing residual 1064 nm output from the laser into water. Sample and reference beams were focused onto the entrance slits of a Spex spectrograph equipped with a 532 nm notch filter and analyzed with a Princeton image-intensified, dual-diode array optical recorder. The signals were transferred to a microcomputer for storage and analysis with approximately 300 individual laser shots being averaged for each determination.

Electrochemical measurements were made by cyclic voltammetry using a BAS CV-50W voltammetric analyzer equipped with a Pt microdisk working electrode and a Ag wire counter electrode. Ferrocene was used as an internal standard and was calibrated against a saturated calomel reference electrode (SCE) separated from the electrolysis cell by a glass frit presoaked with electrolyte solution. Solutions contained the electrode-active material (ca. 2×10^{-4} M) in deoxygenated acetonitrile containing tetra-*N*-butylammonium hexafluorophosphate (0.1 M). The quoted half-wave potentials were reproducible to ±10 mV.

Titrations were made by adding known aliquots of a concentrated deoxygenated acetonitrile solution of a salt to a deoxygenated solution of the calix[4]arene in acetonitrile containing tetra-*N*-butylammonium perchlorate (0.1 M). The course of reaction was followed by recording the luminescence spectrum after each addition, under 514 nm excitation. The luminescence intensity was measured at 50 different wavelengths across the region 610−760 nm, and a total of 40 additions were made for each system examined. The titration data were analyzed by global methodology using the SPECFIT program. The quoted stability constants were found to be reproducible to within 7%.

Computational Studies. All systems were simulated in acetonitrile solution for at least 500 ps. Following from the NMR results, the cone, paco, and 1,3-alt *syn*-aryl forms were considered for **Ru(Q)** and **Ru2(Q)** while the corresponding Ba^{2+} complexes were built only in the cone conformation. Charge neutrality was achieved by adding two ClO_4^- counterions per Ru^{II} and Ba^{2+} atom. Calculations were performed with the AMBER4.1 package[34] for MM and MD simulations using the following representation of the potential energy:

$$E_T = \sum_{\text{bonds}} (r - r_{eq})^2 + \sum_{\text{angles}} K_q(\theta - \theta_{eq})^2 + \sum_{\text{dihedrals}} V_n(1 + \cos(n\theta - \gamma)) + \sum_{i<j} \left[\frac{B_{ij}}{R_{ij}^{12}} - \frac{A_{ij}}{R_{ij}^{6}} + \frac{q_i q_j}{\epsilon R_{ij}} \right]$$

Interactions involving the Ba^{2+} and Ru^{II} cations and all nonbonded interactions were depicted by a 1−6−12 potential, where electrostatic forces are approximated by Coulombic effects. In most cases, the AMBER force field[35] was used with the atom types being defined in Figure S1 in the Supporting Information. The van der Waals ϵ and R^* parameters for Ba^{2+} were taken from Åqvist.[36] The R^* radius of Ru^{II} (0.72 Å) was fitted in order to reproduce the experimental Ru···N distance of 2.06 Å in $[Ru(bpy)_3]^{2+}$, taking $\epsilon = 0.875$ kcal mol^{-1} as for Mg^{2+}.[36]

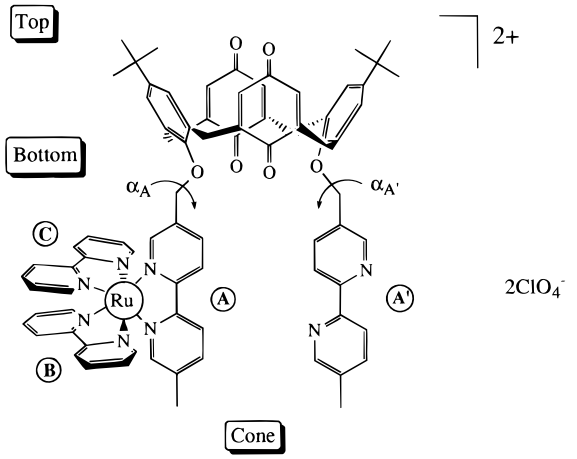

Figure 1. Pictorial representation of **Ru(Q)** and definition of parameters used for the MD simulations. The angles between the average planes of opposite phenolic and opposite quinoid rings are $\omega_{AA'}$ and $\omega_{QQ'}$, respectively.

Atomic charges (given in Figures S2 and S3 in the Supporting Information) were derived from electrostatic potentials calculated with the SPARTAN software.[37] To model the calix[4]arene and the "free" bpy moieties, two sets of calculations were performed at the 6-31G* level. First, *cis*-bpy, quinone, and anisole molecules in their free state were used to depict **Ru_2(Q)** and **Ru(Q)** in the absence of barium perchlorate. The second set of calculations, being performed on the Mg^{2+} complexes of these molecules, was used to simulate the **Ru_2(Q)**Ba^{2+} and **Ru(Q)**Ba^{2+} complexes, where Mg^{2+} was fixed at 2.8 Å from O (quinone), 3.3 Å from O (anisole), and 3.1 Å from N (bpy), respectively. The charges on the $[Ru(bpy)_3]^{2+}$ fragment were obtained from a 3-21G ab initio calculation. We note that the metal center has a charge of +1 since an electron has been transferred from the three bipyridine ligands to the metal, while the total charge of the $[Ru(bpy)_3]^{2+}$ fragment remains +2.0. In the AMBER calculations, the Ru···N distances were constrained at 2.06 Å and the N−Ru−N angles were maintained at 90°. The acetonitrile molecules were represented explicitly with the OPLS model.[38] The solvent box was "cubic", ca. $60 \times 50 \times 50$ Å^3, containing ca. 1600 CH_3CN molecules. Periodic boundary conditions, with a residue-based twin cutoff of 10/15 Å, were used to calculate nonbonded interactions.

The MD simulations were performed in the (N, P, T) ensemble. The solute and solvent were coupled separately to a temperature bath[39] of 300 K with a coupling constant of $\tau_T = 0.2$ ps. The equations of motion were integrated with a time step Δt of 1 fs, starting with random velocities. The C−H bonds of the solute and all bonds of the solvent molecules were kept rigid using SHAKE. After a conjugate gradient energy minimization, initial MD simulations were run for 20 ps, keeping the solute frozen (including the ClO_4^- counterions). This step was followed by free MD simulations over 500 ps duration. Analysis of the results was performed from the trajectories which were saved at intervals of 1 ps.

The **Ru(Q)** system contains four bipyridine units which are referred to as bpy_A and $bpy_{A'}$, these being attached to the lower rim of the calix[4]arene by a methylene bridge, while bpy_B and bpy_C are coordinated to the Ru^{2+} cation (Figure 1). Starting structures of the **Ru(Q)**Ba^{2+} and **Ru_2(Q)**Ba^{2+} complexes were built with the MACROMODEL sofware,[40] assuming a cone conformation of the calix[4]diquinone. The Ba^{2+} cation was initially placed on the C_2 symmetry axis of the cone, centered ca. 3 Å from each of the four surrounding oxygen atoms of **Ru(Q)**, while the two appended bipyridine arms bpy_A and $bpy_{A'}$ were positioned in an "axial orientation". Two ClO_4^- counterions were added

(34) Pearlman, D. A.; Case, D. A.; Caldwell, J. W.; Ross, W. S.; Ferguson, D. M.; Seibel, G. L.; Singh, U. C.; Weiner, P. K.; Kollman, P. A. *AMBER4.1*; University of California: San Francisco, 1995.

(35) Kollman, P. A.; Caldwell, J. W.; Fox, T.; Spellmeyer, D. C.; Ferguson, D. M.; Merz, K. M.; Gould, I. R.; Bayly, C. I.; Cieplak, P.; Cornell, W. D. *J. Am. Chem. Soc.* **1995**, *117*, 5179.

(36) Åqvist, J. *J. Phys. Chem.* **1990**, *94*, 8021.

(37) Version 4.0.4, S. V. Wave Function Inc. 1995.

(38) Jorgensen, W. L.; Briggs, J. M. *Mol. Phys.* **1988**, *63*, 547.

(39) Berendsen, H. J. C.; Postma, J. P. M.; van Gunsteren, W. F.; DiNola, A. *J. Chem. Phys.* **1984**, *81*, 3684.

(40) Mohamadi, F.; Richards, N. G.; Guida, W. C.; Liskamp, R.; Lipton, M.; Caufield, C.; Chang, G.; Hendrickson, T.; Still, W. C. *J. Comput. Chem.* **1990**, *11*, 440.

Scheme 1

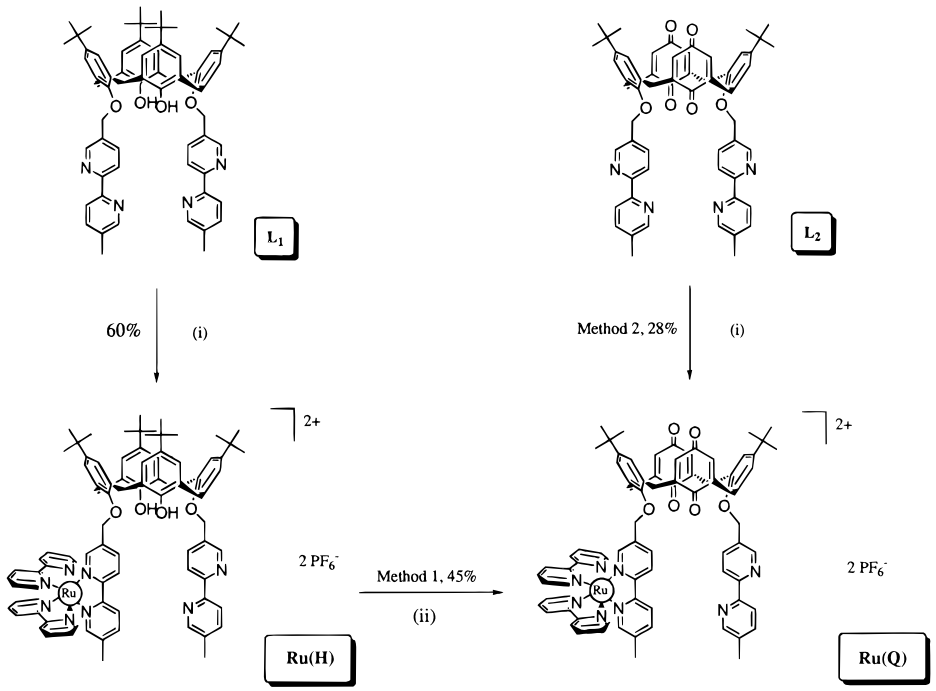

around the $[Ru(bpy)_3]^{2+}$ fragment. For the two other ClO_4^- anions, we considered two alternative starting positions in which the anions were, respectively, in contact with Ba^{2+} ($Ba^{2+}\cdots Cl = 4.5$ Å) or remote (at 11 Å). Upon energy minimization, the "free" bipyridine arm $bpy_{A'}$ remained axial but moved to Ba^{2+}, leading to two $Ba^{2+}\cdots N(bpy)$ contacts of ca. 3 Å. The uncomplexed states of **Ru(Q)** and **Ru$_2$(Q)** were obtained by removing $Ba(ClO_4)_2$ from the Ba^{2+} complexes in the cone conformation. The paco and 1,3-alt forms, respectively, were obtained by flipping one and two quinones. In all systems, the Ru^{II} atom remains surrounded by three bipyridines and in loose contact with the two ClO_4^- counterions ($Ru^{II}\cdots Cl$ distances range from 7.5 to 10.0 Å) but well shielded from the solvent. The closest CH_3CN molecules have their N atom directed toward the Ru^{II} center and are located 5.7 Å from the metal center.

Results and Discussion

Synthesis. The monoruthenium complexes of podands **L$_1$** and **L$_2$** were prepared using two different synthetic protocols, as illustrated in Scheme 1. First, ligand **L$_1$**[29] was allowed to react with 1 equiv of $[Ru(bpy)_2Cl_2]\cdot 2H_2O$, giving the required **Ru(H)** in 60% yield. Subsequent oxidation with thallium(III) in acid media[41,42] afforded the corresponding **Ru(Q)** complex in 45% yield. No ruthenium(III) complex was isolated during the oxidation step. The second procedure consists of complexing one pendant bipyridine unit of the calix[4]diquinone ligand **L$_2$**[30] with 1 equiv of $[Ru(bpy)_2Cl_2]\cdot 2H_2O$. The diruthenium complexes **Ru$_2$(H)** and **Ru$_2$(Q)** of ligands **L1** and **L2** were prepared using the same experimental procedures but with a slight excess of the ruthenium precursor (Chart 1). It is important to note that the quinoid functions in these systems are stable over prolonged storage in the solid state and for considerable time in solution. This enables isolation of particularly "clean" samples, free from contamination by the corresponding hydroquinol derivatives, for examination by photophysical methods. Related deuterated complexes were prepared usng perdeuterated ruthenium(II) precursors (Chart 1).

Photophysical Properties of the Ruthenated Calix[4]arenes. Absorption spectra recorded for the various ruthenated calix[4]arenes, both phenolic and quinone derivatives, are dominated by intense metal-to-ligand, charge-transfer (MLCT) transitions associated with the ruthenium(II) tris(2,2′-bipyridyl) fragments (Figure 2a). For each compound, the absorption maximum (λ_{max}) of the MLCT band is around 450 nm with the molar extinction coefficient (ϵ_{max}) measured at the absorption peak being ca. 15 000 M^{-1} cm^{-1} per metal center (Table 1). Absorption bands due to the carbonyl groups of the quinone functions are hidden by the more intense MLCT transitions, but the π,π^* transitions localized on the various aromatic units are clearly visible at $\lambda < 300$ nm. Weak luminescence (Figure 2b) could be detected at long wavelength for the phenolic-derived compounds **Ru(H)** and **Ru$_2$(H)**, with the emission maximum (λ_{lum}), quantum yield (Φ_{lum}), and lifetime (τ_L) measured in deoxygenated acetonitrile remaining close to those measured for the parent complex (Table 1). It is clear that the calix[4]arene platform does not quench the lowest-energy excited triplet state of the ruthenium(II) tris(2,2′-bipyridyl) fragment in these compounds. However, luminescence from the corresponding calix[4]diquinones **Ru(Q)** and **Ru$_2$(Q)** is greatly attenuated (Figure 2b), even though there are no apparent spectral shifts (Table 1), indicating that the electron-affinic quinone moieties act as quenchers for the triplet state of the appended metal complex. Other studies made with molecular dyads[20] formed by covalent attachment of a quinone to ruthenium(II) tris(2,2′-bipyridyl) and for appropriate bimolecular systems[43] indicate that luminescence quenching is most likely due to light-induced electron transfer from the metal center to the quinone. Triplet energy transfer, which is thermodynamically uphill by ca. 0.2 eV, is considered less likely than electron

(41) McKillop, A.; Swann, B. P.; Taylor, E. C. *Tetrahedron* **1970**, *26*, 4031.

(42) Reddy, P. A.; Koshyap, R. P.; Watson, W. M.; Gutsche, C. D. *Isr. J. Chem.* **1992**, *32*, 89.

(43) (a) Darwent, J. R.; Kalyanasundaram, K.; Porter, G. *J. Chem. Soc., Faraday Trans. 2* **1981**, *77*, 373. (b) Planchard, D.; Vos, J. G.; von Zelewsky, A. *J. Photochem.* **1987**, *36*, 267.

Chart 1

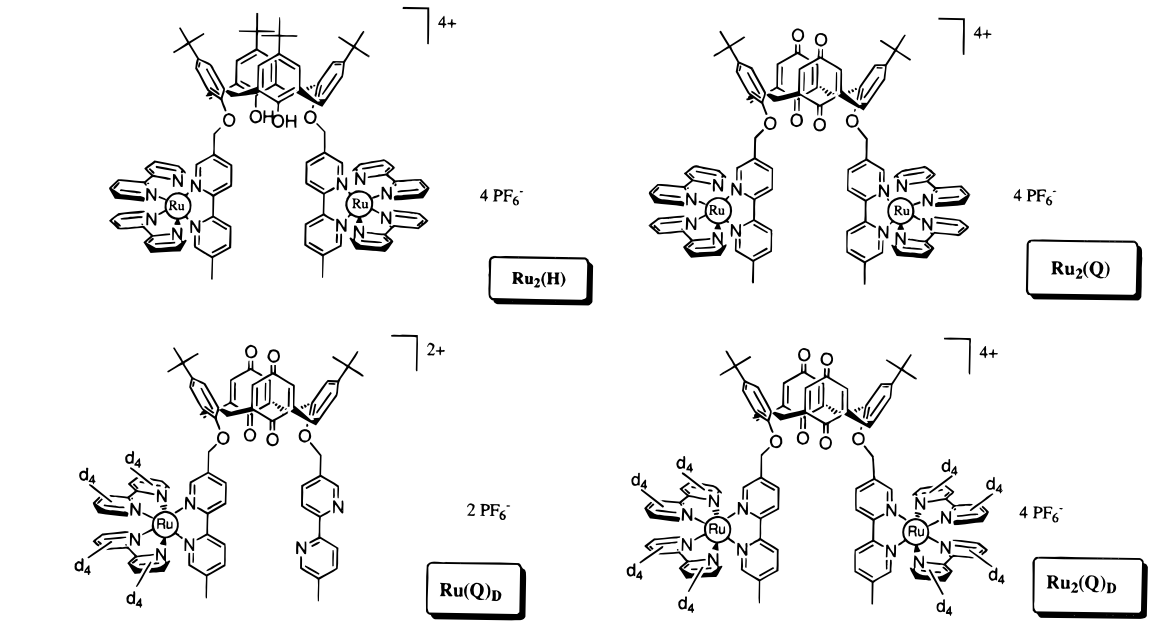

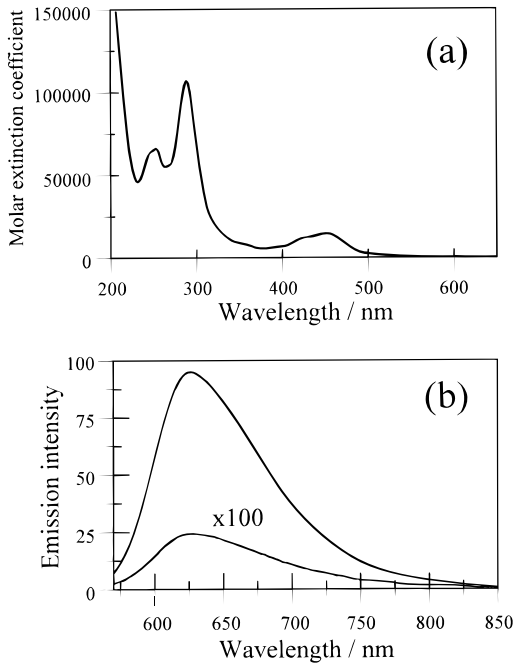

Figure 2. (a) Absorption spectrum recorded for **Ru(Q)** in acetonitrile solution. (b) Comparison of emission spectra recorded for **Ru(H)** and **Ru(Q)** in deoxygenated acetonitrile, with the latter spectrum being shown at 100× amplification for clarity of presentation.

transfer, and laser flash photolysis studies failed to detect the quinone triplet state as an intermediate.

Cyclic voltammograms recorded for the various ruthenated calix[4]arenes in acetonitrile show a quasi-reversible wave on anodic scans corresponding to one-electron oxidation of the appended metal center. There is no indication of electronic coupling between the metal centers in **Ru_2(H)** or **Ru_2(Q)**, and the derived half-wave potentials (E_{ox}) show no obvious dependence on molecular structure (Table 2). Furthermore, these E_{ox} values remain comparable to those recorded for simpler analogues and show only slight modification upon oxidizing the phenol to the quinone. Oxidation peaks due to the phenolic subunits are not observed in the cyclic voltammograms, at least at potentials less than 1.4 V vs SCE. On cathodic scans, a series

Table 1. Photophysical Properties of the Various Calix[4]arene-Derived Species and Their Barium Complexes As Measured in Deoxygenated Acetonitrile at 20 °C

compd	λ_{max}/nm[a]	ϵ_{max}[b]	λ_{lum}/nm[c]	Φ_{lum}[d]	τ_L/ns[e]
$[Ru(bpy)_3]^{2+}$	452	14 700	625	0.062	980
Ru(H)	451	13 600	625	0.085	1100
Ru(Q)	451	14 400	630	0.0004	6.1[f]
Ru(Q)Ba^{2+}	451		635	0.057	740
Ru_2(H)	452	37 400	627	0.081	1120
Ru_2(Q)	452	29 500	630	0.0002	2.3[f]
Ru_2(Q)Ba^{2+}	452		630	0.062	880

[a] Absorption maximum, ±2 nm. [b] Molar extinction coefficient measured at the maximum of the MLCT transition, ±5%. [c] Emission maximum, ±5 nm. [d] Emission quantum yield, ±15%. [e] Triplet lifetime, ± 5%. [f] Lifetime measured by transient absorption spectroscopy since the time-resolved emission decay profile was nonexponential.

of three quasi-reversible reduction peaks can be resolved that correspond to successive addition of an electron to each of the coordinated bpy ligands. The derived half-wave potentials (E_{red}) remain similar to those recorded for the parent complex (Table 2).

Additional reduction peaks are seen in the cyclic voltammograms recorded for **Ru(Q)** and **Ru_2(Q)** which can be attributed to reduction of the quinoid moieties. In each case, two broad peaks are observed centered around −0.7 and −1.5 V vs SCE. which correspond, respectively, to formation of the π-radical anion and the π-dianion (Table 2). The broadness of these peaks arises because the two quinoid walls of each calix[4]arene macrocycle are reduced at slightly different potentials because of Coulombic effects associated with their close spacing. It is difficult, therefore, to derive accurate half-potentials for one-electron reduction of the quinone moieties.

On the basis of the electrochemical and luminescence spectral measurements, it appears that there is a small thermodynamic driving force ($\Delta G°$) for light-induced electron transfer in the quinone-bearing systems but not in the corresponding phenolic derivatives (Table 2). These driving forces were calculated according to

$$\Delta G° = E_{ox} - E_{red} - E_T + \Delta E_C$$

Table 2. Electrochemical Properties of the Various Calix[4]arene-Derived Species As Measured in Acetonitrile at 20 °C with Tetra-*N*-butylammonium Hexafluorophosphate (0.1 M) as Supporting Electrolyte and the Corresponding Thermodynamic Driving Forces for Light-Induced Electron Transfer from the Triplet State of the Ruthenium(II) Tris(2,2′-bipyridyl) Fragment to the Calix[4]arene Platform

compd	E_{ox}[a]	E_{red}[b]	$\Delta G°$/eV[c]
$[Ru(bpy)_3]^{2+}$	1.27 (70)	−1.35 (75), −1.54 (80), −1.79(80)	
Ru(H)	1.35 (70)	−1.43 (80), −1.62 (80), −1.94 (80)	>0.6
Ru(Q)	1.22 (72)	−0.73 (72), −1.36 (100), −1.54 (80), −1.62 (71), −1.86 (100)	−0.26
Ru(Q)Ba^{2+}		−0.59 (irr)	−0.31
Ru_2(H)	1.25 (90)	−1.44 (76), −1.63 (76), −1.93 (98)	>0.5
Ru_2(Q)	1.12 (98)	−0.76 (60), −1.45 (98), −1.50 (irr), −1.63 (86), −1.95 (104)	−0.33
Ru_2(Q)Ba^{2+}			

[a] Oxidation potential, V vs SCE (measured with ferrocene as internal standard, E_{ox} = 0.32 V vs SCE, ΔE_p = 64 mV), ±15 mV, the splitting between anodic and cathodic peaks is given in parentheses. [b] Reduction potential, V vs SCE, ±15 mV. Irr means irreversible. [c] Thermodynamic driving force for light-induced electron transfer, ±0.03 eV.

$$\Delta E_C = \Delta Z e^2/4\pi\epsilon_0\epsilon_S R \quad (1)$$

where E_T is the electronic energy of the triplet state localized on the metal complex, ΔZ is the difference in electronic charge between radical pair and initial reactants, ϵ_S is the static dielectric constant of the solvent, and R is the distance between the center of the ruthenium cation and the center of the quinone within the encounter complex. In making these calculations, it was assumed that electron transfer takes place preferentially at orbital contact[44] so that R is assigned a tentative value of 8 Å. While the derived $\Delta G°$ values appear consistent with the extent of emission quenching noted for **Ru(Q)** and **Ru_2(Q)**, laser flash photolysis studies did not resolve the intermediate formation of a radical ion pair. Instead, there is evidence only for the rapid (i.e., within the laser pulse) formation and slower decay of the triplet state of the ruthenium(II) tris(2,2′-bipyridyl) fragment (Figure 3). Such behavior is common for donor−acceptor systems formed from quinones[45] and is indicative of charge recombination ($\Delta G° \approx -1.9$ eV) being much faster than charge separation.[46]

According to the transient absorption studies, decay of the triplet excited states localized on the ruthenium(II) tris(2,2′-bipyridyl) fragments in **Ru(Q)** and **Ru_2(Q)** could be approximated to first-order kinetic processes (Figure 3b,c). The triplet lifetimes derived from these kinetic fits were markedly shorter than those measured for the corresponding phenolic derivatives (Table 1). However, time-resolved emission studies, which are considerably more precise than transient absorption techniques, showed that these triplets decayed via nonexponential kinetics (Figure 4). This is in marked contrast to the situation found for **Ru(H)** and **Ru_2(H)** where decay profiles are strictly monoexponential (Figure 4). Nonexponential decay profiles are often observed in photoactive dyads in which the reactants are connected by a flexible chain,[47] where they can be attributed to diffusive motion of luminophore and quencher within the excited-state lifetime. The rate of electron transfer is expected to increase for shorter separations[44] and, at a fixed distance, to depend on mutual orientation of donor and acceptor.[48] Despite

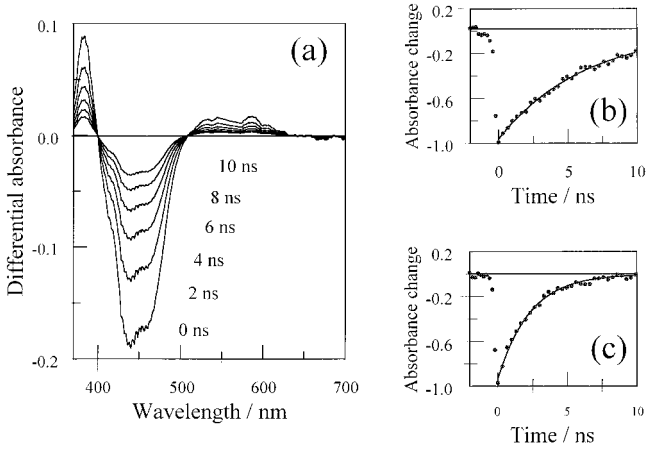

Figure 3. (a) Transient differential absorption spectra recorded at various delay times after excitation of **Ru(Q)** in deoxygenated acetonitrile with a 20-ps laser pulse at 532 nm. (b) Kinetic profile showing the recovery of ground-state **Ru(Q)**, as measured at 450 nm, with the solid line drawn through the data points representing a nonlinear, least-squares fit to a first-order process with a lifetime of 6.1 ns. (c) Kinetic profile showing the recovery of ground-state **Ru_2(Q)**, as measured at 450 nm, with the solid line drawn through the data points representing a nonlinear, least-squares fit to a first-order process with a lifetime of 2.3 ns.

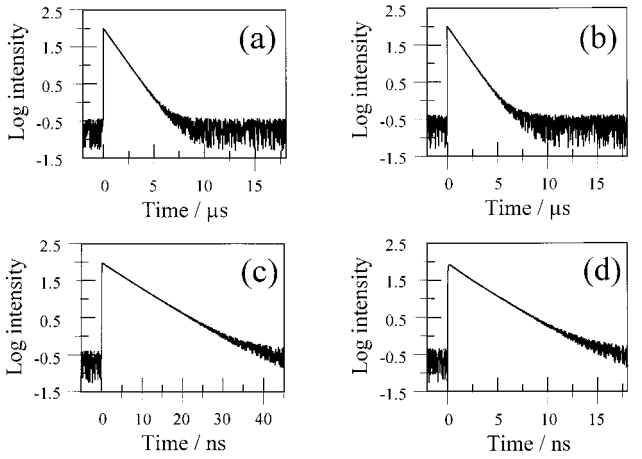

Figure 4. Time-resolved emission decay profiles measured at 630 nm following laser excitation at 532 nm for (a) **Ru(H)**, (b) **Ru_2(H)**, (c) **Ru(Q)**, and (d) **Ru_2(Q)** in deoxygenated acetonitrile at 20 °C.

the short connecting chains used in the present investigation, examination of a space-filling molecular model suggested that **Ru(Q)** could adopt a multitude of conformations in which the mutual positioning of the donor−acceptor functions varies considerably. The situation for **Ru_2(Q)** seemed to be simpler in that electrostatic repulsion between chromophoric units might

(44) (a) Brocklehurst, B. *J. Phys. Chem.* **1979**, *83*, 536. (b) Miller, J. R.; Beitz, J. V. *J. Chem. Phys.* **1981**, *74*, 6746. (c) Siders, P.; Cave, B. J.; Marcus, R. A. *J. Chem. Phys.* **1984**, *81*, 5613.

(45) (a) Mataga, N. *Pure Appl. Chem.* **1984**, *56*, 1255. (b) Mataga, N.; Karen, A.; Okada, T.; Nishitani, S.; Kurata, N.; Sakata, Y.; Misumi, S. *J. Am. Chem. Soc.* **1984**, *106*, 2442. (c) Mataga, N.; Karen, A.; Okada, T.; Nishitani, S.; Sakata, Y.; Misumi, S. *J. Phys. Chem.* **1984**, *88*, 4650.

(46) The rate of charge recombination becomes much slower in nonpolar solvents, such as benzene, because of the increased driving force and reduced reorganization energy. For details, see: Mataga, N.; Miyasaka, H. *Prog. React. Kinet.* **1994**, *19*, 317.

(47) (a) Harriman, A. *Pure Appl. Chem.* **1990**, *62*, 1107. (b) Mataga, N.; Yao, H.; Okada, T.; Kanda, Y.; Harriman, A. *Chem. Phys.* **1989**, *131*, 473. (c) Indelli, M. T.; Bignozzi, C. A.; Harriman, A.; Schoonover, J. R.; Scandola, F. *J. Am. Chem. Soc.* **1994**, *116*, 3768.

be expected to enforce an extended geometry.[49] More detailed structural studies, however, were undertaken with a view to clarifying the nature of the ground-state species.

Structure of the Ruthenated Calix[4]arenes. For the purpose of the present investigation, there are two features of the ground-state structure of the functionalized calix[4]arenes that need to be understood before a meaningful interpretation of the photophysical data can be attempted. The most important issue concerns the geometrical relationship between the pendant $[Ru(bpy)_3]^{2+}$ fragment(s) and the quinoid walls of the macrocycle since this establishes the electron-transfer pathway. It is particularly important to evaluate the possibility of direct contact between the quinones and coordinated bpy ligands on the luminophoric group. In the event that these subunits come into orbital contact within the inherent lifetime of the luminophore (e.g., 1 μs) intramolecular diffusional quenching[50] is likely to compete with through-bond electron transfer because the connecting chain is not a good conduit for electronic processes.[51] A related conformational concern is the shape and mobility of the macrocycle, and prior work on nonmetalated calix[4]-diquinones found[41,52] that paco conformations predominate in solution at ambient temperature, depending on the nature of the solvent. In fact, it appears that the quinoid walls can rotate about the connecting methylene groups.[25] Such behavior would complicate analysis of the electron-transfer kinetics inasmuch as it is well-known that the rate of electron transfer depends critically on mutual orientation of the reactants.[48] To address these two issues, it has been necessary to undertake a series of NMR studies, including the use of deuterated analogues that simplify the spectra, and to perform molecular-dynamics simulations that provide critical information about the positioning of the pendant luminophore(s).

Both **Ru(H)** and **Ru_2(H)** were found to adopt a distorted-cone conformation in solution.[53,54] Close examination of the ^{1}H NMR spectra recorded for these complexes reveals that the bridging methylene groups of the calix[4]arene platform appear as a set of four well-defined AB quartets. As expected, the ^{1}H NMR spectrum of **Ru(H)** exhibits a characteristic single AB quartet for the bpy$-CH_2-$O group complexed to the chiral "Ru(bpy)$_2$" moiety and a singlet for the uncomplexed bpy$-CH_2-$O fragment. For **Ru_2(H)**, two AB systems are observed for the bridging methylene H-atoms of the Ar$-$O$-CH_2-$bpyRu(bpy)$_2$ subunits. ^{13}C NMR spectra recorded for **Ru(H)** and **Ru_2(H)** show two signals for the bridging methylene groups in the region between 35.0 and 33.9 ppm. Such behavior is clearly indicative of a cone structure for the calix[4]arene macrocycle.[53,54] Furthermore, since four AB systems are present for the bridging methylene groups in the ^{1}H NMR spectra, we may deduce that the macrocycle is distorted.

For the corresponding diquinone species the situation is more complex. In particular, the ^{1}H NMR spectrum recorded for **Ru(Q)** exhibits three signals (integration 2/1/1) for the quinoid functions and two signals (integration 9/9) that are clearly associated with the terminal *tert*-butyl groups. To clarify interpretation of these results, it was necessary to simplify the spectra, and this was achieved by deuterating the two bpy ligands not directly attached to the calix[4]arene and by varying the temperature. Deuteration of the coordinated bpy's greatly simplifies the aromatic part of the spectrum, giving rise to a 12- and 6-H-atom pattern, respectively, for **Ru(Q)$_D$** and **Ru_2(Q)$_D$**. Upon decreasing the temperature, the quinone signals observed for **Ru(Q)$_D$** coalesce into two broad singlets at 268 K whereas the two signals due to the *tert*-butyl groups coalesce into a large singlet at 280 K. Activation energies for coalescence (ΔG_C) of 56 and 69 kJ mol^{-1}, respectively, were estimated for the quinoid and *tert*-butyl functions from the following expression:

$$\Delta G_C = RT_C(22.96 + \ln(T_C/\Delta\nu)) \qquad (2)$$

where T_C is the coalescence temperature and $\Delta\nu$ is the difference in frequency between the two peaks.[55] Previous investigations made with related calix[4]diquinones have shown that, at ambient temperature, the quinoid moieties rotate[25,52] through the cavity defined by the macrocycle. Consequently, we attribute the temperature dependence noted here for the quinone signals to internal rotation about the bridging methylene groups. This dynamic process is inhibited at low temperature, and in frozen media **Ru(Q)$_D$** adopts a cone conformation.[56,57] In contrast, the bulky *tert*-butyl-containing rings remain static with respect to each other (*syn*-aryl conformation).[25] At room temperature, therefore, the macrocycle comprises different conformations (*syn*-cone, *syn*-paco and *syn*-1,3-alt). In both ruthenium complexes, the aryl substituents [O$-CH_2-$bpyRu(bpy)$_2$, O$-CH_2-$bpy, and *tert*-butyl groups] impose a *syn*-bpy conformation, which is not inverted during complexation.

More information about the average conformations of these functionalized calix[4]diquinones was sought from sophisticated molecular-dynamics simulations. During the dynamics, each of the starting conformations (cone, paco, or 1,3-alt) was retained but displayed significant fluctuations with respect to the shape of the calixarene moiety and of the pendant bpy arms. Evolution of the calixarene structure is conveniently characterized by the angles $\omega_{AA'}$ between the opposite phenols and $\omega_{QQ'}$ between opposite quinones. Their average values are reported in Table S1. The phenols are almost coparallel ($\omega_{AA'}$ ranges from 10 to 60°) in all cases except for **Ru_2(Q)** where $\omega_{AA'}$ is about 120 ± 15°. The angle $\omega_{QQ'}$ is also less than 60° in the cone and alt forms, but reveals a nearly perpendicular arrangement ($\omega_{QQ'}$ = 120°) in the two paco ligands. In all structures, the quinones are much more mobile than the phenolic rings, and may instantaneously adopt conformations which sit on the pathway for interconverting from cone to paco or from paco to alt forms. Schematically, the pendant bpy arms are more or less diaxial, as the average α_A and $\alpha_{A'}$ angles range from 145 to 190° in the

(48) (a) Hoffman, R. *Acc. Chem. Res.* 1971, *4*, 1. (b) Hoffman, R.; Imarura, A.; Hehre, W. *J. Am. Chem. Soc.* **1968**, *90*, 1499. (c) Closs, G. L.; Miller, J. R. *Science* **1988**, *240*, 440. (d) Oevering, H.; Verhoeven, J. W.; Paddon-Row: M. N.; Warman, J. M. *Tetrahedron* **1989**, *45*, 4751. (e) Oliver, A. M.; Craig, D. C.; Paddon-Row: M. N.; Kroon, J.; Verhoeven, J. W. *Chem. Phys. Lett*. ***1988***, *150*, 366. (f) Sakata, Y.; Tsue, H.; O'Neil, M. P.; Wiederrecht, G. P.; Wasielewski, M. R. *J. Am. Chem. Soc.* **1994**, *116*, 6904.

(49) (a) Ryu, C. K.; Wang, R.; Schmehl, R. H.; Ferrere, S.; Ludwikow, M.; Merkert, J. W.; Headford, C. E. L.; Elliott, C. M. *J. Am. Chem. Soc*. **1992**, *114*, 430. (b) Yonemoto, E. H.; Riley, R. L.; Kim, Y. I.; Atherton, S. J.; Schmehl, R. H.; Mallouk, T. E. *J. Am. Chem. Soc*. **1992**, *114*, 8081.

(50) In fluid solution, it is often considered that bimolecular electron transfer proceeds only at orbital contact, by way of a precursor complex, but recent models indicate that noncontact electron transfer cannot be neglected. For details, see: Burshtein, A. I.; Shokhirev, N. V. *J. Phys. Chem. A* **1997**, *101*, 25.

(51) Benniston, A. C.; Harriman, A.; Grosshenny, V.; Ziessel, R. *New J. Chem*. **1997**, *21*, 405.

(52) Beer, P. D.; Chen, Z.; Gale, P. A. *Tetrahedron* **1994**, *50*, 931.

(53) Gutsche, C. D.; Bauer, L. J. *J. Am. Chem. Soc*. **1985**, *107*, 6052.

(54) Jaime, C.; De Mendoza, J.; Prados, P.; Nieto, P. M.; Sànchez, C. *J. Org. Chem*. **1991**, *56*, 3372.

(55) Derome, A. E. In *Modern NMR Techniques for Chemistry Research*; Pergammon Press: Oxford, 1991.

(56) van Loom, J.;-D.; Ardini, A.; Coppi, L.; Verboom, W.; Pochini, A.; Ungaro, R.; Harkema, S.; Reinhoudt, D. N. *J. Org. Chem*. **1990**, *55*, 5639.

(57) Morita, Y.; Agawa, T.; Nomura, E.; Taniguchi, H. *J. Org. Chem*. **1992**, *57*, 3658.

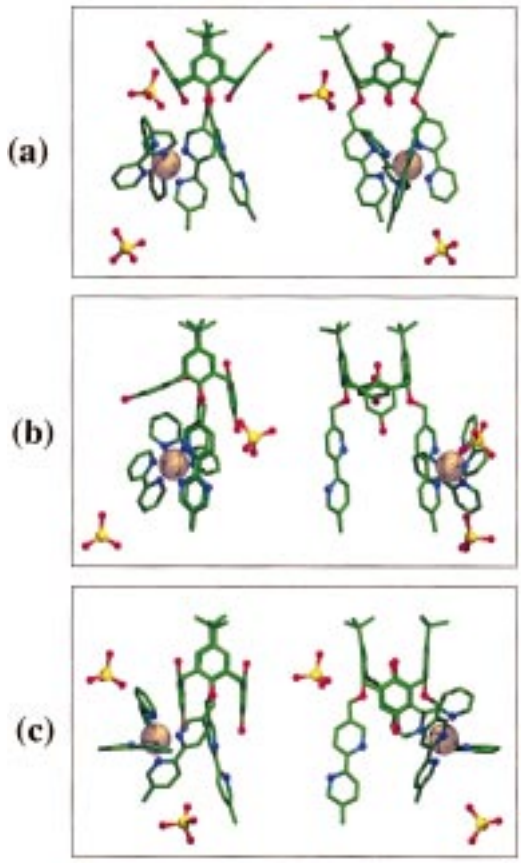

Figure 5. Typical orthogonal views of the simulated structures of **Ru(Q)** in acetonitrile: (a) cone at 500 ps, (b) paco at 500 ps, (c) 1,3-alt at 300 ps.

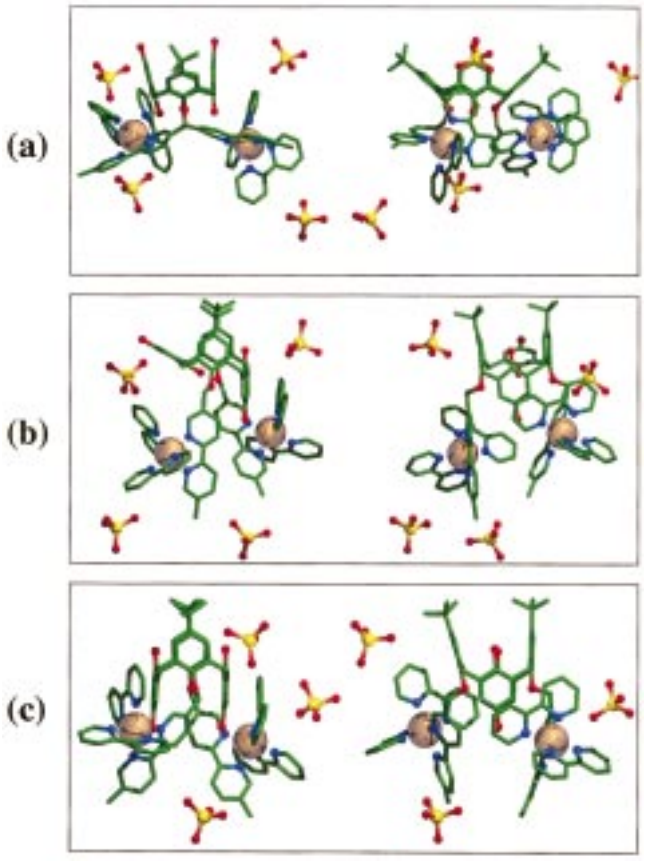

Figure 6. Typical orthogonal views of the simulated structures of **Ru_2(Q)** in acetonitrile: (a) cone at 500 ps, (b) paco at 500 ps, (c) 1,3-alt at 830 ps.

three forms of **Ru(Q)** and in the alt form of **Ru_2(Q)**. In the cone and paco forms of **Ru_2(Q)** these two bpy's are more mobile and oscillate between axial and equatorial orientations. Examination of the cone/paco/alt ligands during the dynamics revealed a marked conformation dependent proximity and stereochemical relationship between some bpy units and quinones. To quantify this proximity, we calculated two sets of parameters, namely, the distances between each proton resident on the coordinated bpy units and the closest quinoid oxygen atoms ($H_{pyr}\cdots O_Q$) (Figure 1) and the distances between the centers of mass of each pyridine and the quinoid carbonyl group ($CM_{pyr}\cdots CM_{CO}$). These distances are plotted as a function of time in Figures S4 and S5 in the Supporting Information. Snapshots of selected structures are also given in Figures 5 and 6.

A noticeable feature of the two 1,3-alt ligands is the widespread occurrence of structures where some pyridine(s) and carbonyl groups at the bottom of the quinones are in close proximity and adopt a more or less coparallel relationship (Figures 5 and 6). The corresponding $CM_{pyr}\cdots CM_{CO}$ distances fluctuate as a function of time, but several of them are shorter than 3.5 Å for more than 80% of the simulated time (Figure S5). Instantaneously, some atoms of bpy and of quinone units can be as close as 3.0 Å, where π-orbitals of these electron-donating and -accepting groups start to overlap.[58] The shortest $H_{pyr}\cdots O_Q$ distances are ca. 2.6 Å in **Ru(Q)** and in **Ru_2(Q)**, but they are found for structures where the corresponding bpy and quinone moieties are more or less in the same plane, or perpendicular to each other, rather than being cofacial.

The paco forms of **Ru(Q)** and **Ru_2(Q)** also favor proximity between the "inverted quinone" and one bpy, these units lying essentially coparallel. The shortest $CM_{pyr}\cdots CM_{CO}$ distances are ca. 3.5 Å, but the lifetime of these structures is less than in the 1,3-alt form. Short $H_{pyr}\cdots O_Q$ distances are also found in other paco structures (Figure S5). At less than 3 Å, their population is 100% in **Ru(Q)** and 12% in **Ru_2(Q)**, but below 2.5 Å these populations drop to less than 8% in both complexes (Figure S4).

In the two cone forms, the shortest contacts between bpy and quinone units correspond to $CM_{pyr}\cdots CM_{CO}$ distances of 4.5−5.0 Å, which are too large for significant orbital overlap. In addition, their lifetimes are less (about 20%) than those in the 1,3-alt form and they do not display coplanar bpy−quinone arrangements. There are structures having short (i.e., 2.2−2.5 Å) $H_{pyr}\cdots O_Q$ distances whose relative lifetimes are 23% in **Ru(Q)** and 50% in **Ru_2(Q)**, but they do not correspond to "π-stacking" interactions.

The NMR studies and molecular-dynamics simulations confirm that the various calix[4]arenes exist in a state of fluctional motion in solution at ambient temperature. The macrocycle is undergoing dynamic structural distortion on the NMR time scale while the donor−acceptor pair adopts a variety of interconverting conformations. Some of these conformations are highly favorable for electron transfer[48] since the quinone becomes cofacial with one of the bpy ligands coordinated to the metal center, with the two aryl rings lying in close proximity. It seems reasonable to assume that the fastest rates of electron transfer observed for **Ru(Q)** and **Ru_2(Q)** refer to excitation of such conformers present in the ground state, and it is instructive to note that such coparallel arrangements can only be obtained with noncone conformations of the macrocycle. Structural heterogeneity of this type would doubtless account for the

(58) Larsson, S. *J. Am. Chem. Soc.* **1981**, *103*, 4034.

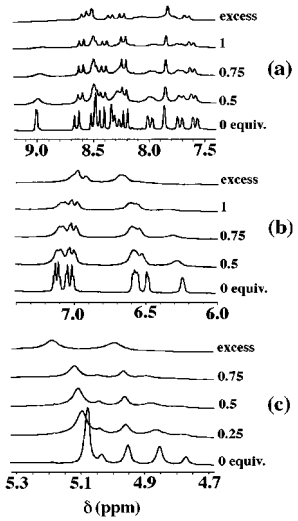

Figure 7. Effect of increasing concentration of $Ba(ClO_4)_2$ on the ^1H NMR spectrum of $\mathbf{Ru(Q)_D}$ (ca. 30 mM) at 25 °C in d_6-acetone: Signals correspond to protons of the (a) nondeuterated bpy, (b) phenolic (LHS) and quinoid (RHS) groups of the calix[4]diquinone, and (c) nonruthenated CH_2-bpy group (singlet) and prochiral CH_2-bpyRu(bpy)$_2$ fragment (AB quartet). Each spectrum corresponds to an increment of 0.25 equiv of $Ba(ClO_4)_2$.

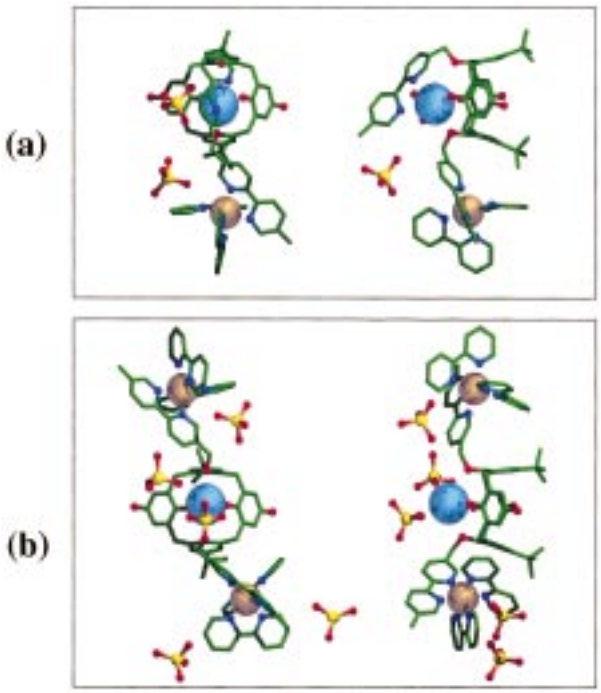

Figure 8. Orthogonal views of the typical structures simulated at 500 ps for the cone forms of (a) **Ru(Q)**Ba and (b) **Ru$_2$(Q)**Ba.

complex kinetics observed for decay of the triplet excited state since each conformation will be characterized by a discrete rate of electron transfer and interconversion of structures can occur within the excited state lifetime. It is especially informative to note the high flexibility of **Ru$_2$(Q)**. This explains the propensity of this species to undergo light-induced electron transfer despite electrostatic repulsion between the pendant chromophores. An obvious feature of this interpretation of the photophysical data is that the decay kinetics should become much simpler if the ground-state structure can be homogenized.

Effect of Barium Perchlorate on the Structure of Ruthenated Calix[4]diquinones. It is known that calix[4]diquinones bind adventitious cations,[59] and in the present system, this could provide a simple strategy by which to constrain the average conformation.[28,60−63] To explore this possibility, additional structural investigations were made with barium perchlorate as the added salt. The effect of increasing concentration of $Ba(ClO_4)_2$ on the ^1H NMR spectrum of $\mathbf{Ru(Q)_D}$ in d_6-acetone is shown in Figure 7 and indicates that complexation takes place. The most pronounced effect is found for the protons resident on the vacant bpy where the 6-line pattern is significantly enhanced. In contrast, addition of $Ba(ClO_4)_2$ has little effect on the bpy signals of $\mathbf{Ru_2(Q)_D}$. Such behavior suggests that the pendant bpy residue is involved in complexation of $Ba(ClO_4)_2$ in $\mathbf{Ru(Q)_D}$. Addition of $Ba(ClO_4)_2$ also modifies the ^1H NMR signals associated with the quinoid functions, and in particular, the 3-line pattern collapses to a singlet. This effect, which is reminescent of the coalescence that takes place on freezing the solvent, indicates that complexation of $Ba(ClO_4)_2$ restricts mobility of the quinoid walls of the macrocyclic cavity.[64] Also apparent in the NMR spectra is the effect of $Ba(ClO_4)_2$ on the diastereoscopic methylene protons of the pendant CH_2-O−bpy arms. Here, the original AB quartet is transformed to a broad singlet (Figure 7). The overwhelming conclusion drawn from these NMR studies is that $Ba(ClO_4)_2$ binds at the lower rim of the calix[4]arene macrocycle where it is held in place by the pendant bpy. Furthermore, the bound cation must reside sufficiently close to the cavity to hinder rotation of each quinoid wall and to repel the adjacent luminophore. The latter effect is visualized by the spectral changes occurring at the CH_2-O−bpy arms where the prochiral methylene protons become directed toward the bound Ba^{2+} cation and are perturbed by the induced electric field.

Again, more information about the ground-state structure was sought from molecular-dynamics simulations made for the ruthenated calix[4]diquinones in the presence of $Ba(ClO_4)_2$. It was found that the Ba^{2+} cation remains bound to the lower rim oxygens, as in the starting structures, throughout the simulation, making shorter contacts with the two O_Q atoms (2.56 ± 0.02 Å) than with the $O_{phenolic}$ atoms (3.10 ± 0.3 Å). For **Ru(Q)**, the two starting positions set for the ClO_4^- counterions converge to a common position where the dissociated anions oscillate at $Cl\cdots Ba^{2+}$ distances of 8−13 Å. For **Ru$_2$(Q)**, an additional ClO_4^- anion, which is shared between Ru^{II} and Ba^{2+}, enters the structure and sits ca. 6.0 Å from the Ba^{2+} cation (Figure 8). Apart from the lower rim oxygen atoms, the vacant bpy contributes to the binding of Ba^{2+} ($Ba^{2+}\cdots N \approx 2.75 \pm 0.10$ Å) in **Ru(Q)** while, in both complexes, the coordination sphere around Ba^{2+} is completed by one or two solvent molecules. The macrocycle retains its cone conformation but is somewhat "pinched" ($\omega_{QQ'} = 80°$ and $\omega_{AA'} = 30°$ in **Ru(Q)** and $\omega_{QQ'} = 100°$ and $\omega_{AA'} = 20°$ in **Ru$_2$(Q)**) and filled by a CH_3CN molecule that remains in dynamic exchange with the solvent bath. The most important feature of these simulations concerns the positioning of the pendant $[Ru(bpy)_3]^{2+}$ fragment(s). During the simulation, these units move from being "axial" (α_A and $\alpha_{A'} = 180°$) to become "equatorial" (α_A and $\alpha_{A'}$ between 0 and 60°), presumably because of electrostatic repulsion by the complexed Ba^{2+} cation. As a result, the bpy ligands coordinated

(59) Beer, P. D.; Gale, P. A.; Chen, Z.; Drew, M. G. B.; Heath, J. A.; Ogden, M. I.; Powell, H. R. *Inorg. Chem.* **1997**, *36*, 5880.
(60) Shinkai, S.; Araki, S.; Kubota, M.; Arimura, T.; Matsuda, T. *J. Org. Chem.* **1991**, *56*, 295.
(61) Iwamoto, K.; Araki, S.; Shinkai, S. *J. Org. Chem.* **1991**, *56*, 4955.
(62) Gomez-Kaifer, M.; Reddy, P. A.; Gutsche, C. D.; Eschegoyen, L. *J. Am. Chem. Soc.* **1994**, *116*, 3580.
(63) Blixit, J.; Detellier, C. *J. Am. Chem. Soc.* **1995**, *117*, 8536.
(64) Gomez-Kaifer, M.; Reddy, P. A.; Gutsche, C. D.; Eschegoyen, L. *J. Am. Chem. Soc.* **1997**, *119*, 5222.

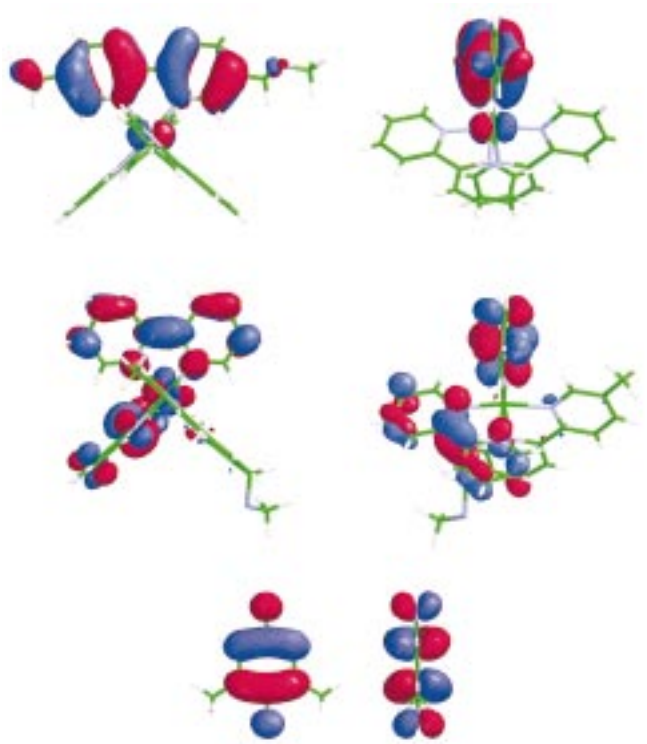

Figure 9. Pictorial representation of the HOMO and LUMO of $[Ru(bpy)_3]^{2+}$ (top) and orthogonal views of the LUMO of benzoquinone (bottom).

to the Ru^{II} center become isolated from the quinoid walls of the calix[4]arene. For **Ru(Q)**, the shortest $H_{pyr}\cdots O_Q$ distances (see Figure S4) are about 5.3 Å while the shortest $CM_{pyr}\cdots CM_{CO}$ separations are 6.5 Å. The corresponding distances for **Ru_2(Q)** are, respectively, 4.0 and 5.5 Å (Figure S5). These distances are too large for orbital overlap between quinone and bpy residues.

Luminescence from the Barium Complexes. The molecular-dynamics simulations indicate that, on the relevant time scale, the initial cone, paco, and 1,3-alt structures are retained. The simulations reveal a conformationally dependent proximity and stereochemical relationship between some of the bpy's that surround Ru^{II} and the quinone groups. In the Ba^{2+} complexes, these groups are too remote (>5 Å) to facilitate electron transfer via orbital overlap. This contrasts with the uncomplexed **Ru(Q)** and **Ru_2(Q)** in the 1,3-alt *syn*-aryl or the paco forms, where some bpy's become essentially parallel to a quinone, allowing for electron transfer to the LUMO π^* orbitals of the quinone. Such a relationship is never observed in the cone form despite short contacts between H_{pyr} protons and O atoms of the quinone. These latter orientations are considered[44] to be less favorable for electron transfer than the cofacial arrangements found in the 1,3-alt or paco forms. Indeed, according to ab initio quantum mechanical calculations made for quinoid and $[Ru(bpy)_3]^{2+}$ fragments, the frontier orbitals are of π type and are delocalized over the bpy and quinone (Figure 9). As a consequence, electronic coupling between the reactants will be considerably enhanced for closely spaced, cofacial orientations but will be much less pronounced for the almost orthogonal structures that abound in the presence of Ba^{2+}. We might expect, therefore, that complexation of Ba^{2+} will decrease the rate of light-induced electron transfer since this both promotes separation of the reactants and destabilizes cofacial orientations. Contrary to this idea, however, is the realization that the bound cation polarizes

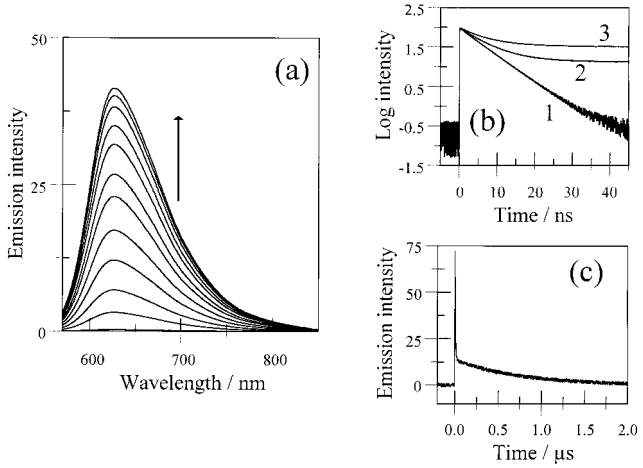

Figure 10. (a) Effect of increasing concentration of barium perchlorate on the emission yield of **Ru(Q)** in deoxygenated acetonitrile solution. (b) Time-resolved emission decay profile recorded for **Ru(Q)** in deoxygenated acetonitrile (1) in the absence of barium perchlorate and in the presence of (2) 10 mM and (3) 32 mM barium perchlorate. (c) Emission decay profile recorded on a long time scale for **Ru(Q)** in the presence of 10 mM barium perchlorate. All solutions contained tetra-*N*-butylammonium perchlorate (0.1 M).

the quinone π-radical anion.[56,62,64,65] This latter effect is apparent from the fact that complexation of Ba^{2+} raises E_{red} by ca. 140 mV[29] and thereby increases $\Delta G°$ for electron transfer from −0.21 to −0.26 eV. Since light-induced electron transfer is likely to occur within the "normal" region of a Marcus rate vs energy gap profile, a small increase in $\Delta G°$ should cause a concomitant increase in rate of electron transfer.[66]

Addition of excess $Ba(ClO_4)_2$ to deoxygenated acetonitrile solutions of **Ru(H)** and **Ru_2(H)** had no apparent effect on the absorption or luminescence spectra, emission quantum yields, or triplet lifetimes. There was no indication that the cation becomes coordinated to the calix[4]arene. In contrast, the presence of $Ba(ClO_4)_2$ enhances the luminescence observed[67] for both **Ru(Q)** and **Ru_2(Q)** in deoxygenated acetonitrile solution (Figure 10a) and causes the appearance of a long-lived component in the decay profiles (Figure 10b). Following excitation with a 20-ps laser pulse at 532 nm, where the appended $[Ru(bpy)_3]^{2+}$ fragments are the only absorbing species present in the system, the decay records could be approximated to the sum of two-exponential components.

$$I(t) = A_1 \exp\left(-\frac{t}{\tau_1}\right) + A_2 \exp\left(-\frac{t}{\tau_2}\right) \qquad (3)$$

Here, the shorter-lived component (τ_1) refers to uncomplexed calix[4]diquinone while the longer-lived species (τ_2) is assigned to the corresponding complex formed upon coordination of Ba^{2+}. For both **Ru(Q)** and **Ru_2(Q)**, τ_1 is on the order of a few nanoseconds while τ_2 is extended to many hundreds of nanoseconds (Table 1). The fractional amplitude of the longer-

(65) Beer, P. D.; Chen, Z.; Drew, M. G. B.; Gale, P. A. *J. Chem. Soc., Chem. Commun.* **1994**, 2207.

(66) It is anticipated that the total reorganization energy (λ_T) accompanying electron transfer is at least 1 eV such that light-induced electron transfer ($-\Delta G° < 0.2\lambda_T$) will take place well within the limits of the Marcus "normal" region. Charge recombination ($-\Delta G° > \lambda_T$) is likely to be much closer to the apex of a Marcus rate vs energy-gap plot. Solely on thermodynamic grounds, complexation of barium perchlorate is expected to increase the rate of forward electron transfer but decrease the rate of charge recombination. This behavior is not observed experimentally.

(67) Hissler, M.; Harriman, A.; Jost, P.; Wipff, G.; Ziessel, R. *Angew. Chem., Int. Ed. Engl.*, in press.

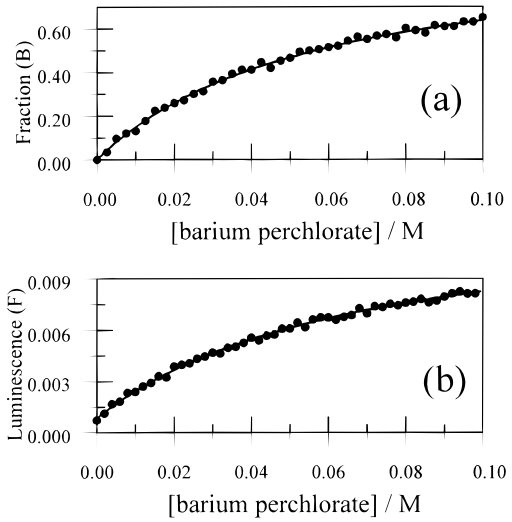

Figure 11. (a) Relationship between the concentration of added barium perchlorate and the fractional contribution of the longer-lived component noted in the time-resolved emission profiles recorded for **Ru(Q)** in deoxygenated acetonitrile solution. The solid curve drawn through the data points (●) corresponds to a nonlinear, least-squares computer fit to a binding constant of 15.5 M^{-1}. (b) Effect of added barium perchlorate on the emission quantum yield measured for **Ru(Q)** in deoxygenated acetonitrile solution. The solid curve drawn through the data points corresponds to a nonlinear, least-squares computer fit to a binding constant of 16.7 M^{-1}. All solutions contained tetra-*N*-butylammonium perchlorate (0.1 M).

lived species (A_2) increases with increasing concentration of added $Ba(ClO_4)_2$, as expected for formation of a 1:1 complex.[15f] In fact, the stability constants (K) for the corresponding Ba^{2+} complexes can be obtained from luminescence titrations (Figure 11) carried out in the presence of tetra-*N*-butylammonium perchlorate (0.1 M):

$$\frac{1}{I_0 - I_L} = \frac{1}{I_0 - I_{lim}} + \frac{1}{K[Ba^{2+}](I_0 - I_{lim})} \qquad (4)$$

where I_L is the observed luminescence intensity, and I_0 and I_{lim} refer, respectively, to the luminescence intensity in the absence of Ba^{2+} and for the corresponding complex formed with Ba^{2+}. The derived parameters are collected in Table 1, and it can be seen that **Ru(Q)** provides the superior binding motif for Ba^{2+} cations. This finding is fully consistent with the indications that the vacant bpy is involved in complexation of the added cation and explains why added Ba^{2+} cations hardly perturb the NMR spectrum recorded for **Ru_2(Q)**. In this latter case, it is likely that complexation of Ba^{2+} to the macrocycle is further inhibited by electrostatic repulsive forces.

The limiting luminescence yields, corresponding to Φ_L for the resultant Ba^{2+} complexes, approach the luminescence quantum yield measured for the phenolic derivatives **Ru(H)** and **Ru_2(H)** (Table 1). This indicates that complexation of a Ba^{2+} cation to the lower rim of the calix[4]diquinone decreases the efficiency of intramolecular electron transfer. The same conclusion is reached by comparing the derived τ_1 and τ_2 values with those measured for the corresponding phenolic derivatives (τ_L). The rate of light-induced electron transfer (k_{ET}), in each system, can be estimated from these lifetimes

$$k_{ET} = \left(\frac{1}{\tau_{1(2)}} - \frac{1}{\tau_L}\right) \qquad (5)$$

and it can be seen that the complexed Ba^{2+} cation causes a 500-fold decrease in rate, despite the slightly improved $\Delta G°$. On the basis of the molecular-dynamics simulations, as augmented by the NMR investigations, this decrease in the rate of light-induced electron transfer can be ascribed to the adoption of extended conformations that preclude significant orbital overlap between a quinone and one of the bpy ligands bound to a Ru^{II} center.

Table 3. Properties of the 1:1 Complexes Formed between a Calix[4]diquinone and a Cation at 20 °C in Deoxygenated Acetonitrile Containing Tetra-*N*-butylammonium Perchlorate (0.1 M) as Background Electrolyte

cation[a]	K/M^{-1} [b]	τ_L/ns[c]	Φ_{lim}[d]	$k_{ET}/10^6\ s^{-1}$ [e]
		Ru(Q)		
		6[f]	0.0002	170
Li^+	420	160	0.013	5.3
Na^+	400	160	0.012	5.3
K^+	185	155	0.012	5.5
Ca^{2+}	22	680	0.052	0.56
Ba^{2+}	16	740	0.055	0.44
Sr^{2+}	12	725	0.054	0.47
La^{3+}	2.1	1020	0.077	0.08
Gd^{3+}	1.7	980	0.074	0.11
Zn^{2+}	2650	2.2[f]	0.0001	455
Zn^{2+}	0.6	690	0.070	0.54
		Ru_2(Q)		
		2[f]	0.0001	500
K^+	21.2	210	0.015	3.9
Ba^{2+}	4.5	880	0.064	0.25
La^{3+}	0.3	1100	0.085	0.02
Zn^{2+}	0.9	650	0.049	0.65

[a] Used as the perchlorate salt, in some cases with water of hydration present. [b] Stability constant for formation of a 1:1 complex measured by steady-state luminescence spectroscopy, ±7%. [c] Triplet lifetime for the cation complex, ±10%. [d] Limiting emission quantum yield extrapolated to complete binding of the cation, ±10%. [e] Rate constant for intramolecular electron transfer in the cation complex, ±15%. [f] Measured by transient absorption spectroscopy.

Complexation of Other Cations. Other cations also bind to **Ru(Q)** in acetonitrile, and although the stability constants vary according to the nature of the cation (Table 3), there is a similar enhancement in luminescence yield and lifetime.[67] Group I (Li^+, Na^+, K^+) and II (Ca^{2+}, Ba^{2+}, Sr^{2+}) cations seem to bind to the calix[4]diquinone in much the same manner[68] since they exert the same effect on the photophysical properties. The binding motif is highly cooperative in such systems in that both bpy and lower rim O atoms are involved in complexation and subsequent screening of the cation. Lanthanide cations (La^{3+}, Gd^{3+}) also restore luminescence from **Ru(Q)**, suggesting that they bind in a similar cooperative manner. The importance of electrostatic repulsion between the reactants becomes clear by comparing k_{ET} values derived for the various cation complexes (Table 3). Thus, monocations give a 30-fold decrease in rate while there is a 300-fold decrease in rate for dications. Intramolecular electron transfer is further curtailed for trications, where the average decrease in rate is ca. 1 700-fold. The same general trend is found for **Ru_2(Q)**, although stability constants tend to be extremely low, but no such effects are seen for the corresponding phenolic derivatives. Qualitatively, these findings are rationalized in terms of the average separation distance being set by Coulombic effects. The receptor, therefore, responds to electronic charge of the cation rather than its chemical identity, and in particular, the triplet lifetime of **Ru(Q)** provides a sensitive measure of this property.

Somewhat different behavior is observed with Zn^{2+}, however, and it appears that two cations are bound at disparate sites. At

(68) Structural studies were not attempted with these other cations, but it is known that complexation of sodium to calix[4]diquinones favors the cone conformation. See refs 62 and 64 for details.

low concentration of zinc perchlorate, efficient cation binding occurs ($K = 2\,650\ M^{-1}$) and is accompanied by extinction of luminescence from the $[Ru(bpy)_3]^{2+}$ fragment. Further increases in the concentration of Zn^{2+} restore luminescence until the final value is close to that found for complexation of Ba^{2+}. This behavior can be rationalized in terms of effective but noncooperative binding of Zn^{2+} at the vacant bpy arm to give a structure somewhat reminescent of **Ru_2(Q)**. If the bound cation acts as the second $[Ru(bpy)_3]^{2+}$ fragment to favor cofacial arrangements between the reactants, this would explain why low concentrations of added Zn^{2+} cause emission quenching.[69] A second Zn^{2+} cation can be coordinated at the lower rim of the calix[4]diquinone platform, with a much reduced binding constant ($K = 0.6\ M^{-1}$), to partially restore emission by conformational control of the superstructure as outlined above for Ba^{2+}. As expected, only one Zn^{2+} cation binds to **Ru_2(Q)** ($K = 0.9\ M^{-1}$) in a manner that restores luminescence.

The systems described here register complexation of a cation by an increase in luminescence yield and lifetime which arise because intramolecular electron transfer is inhibited. A key feature of these prototypes is that electron transfer proceeds via orbital interaction between the redox-active units, involving mutual rotational relaxation, with through-bond "superexchange" interactions[70] playing a less significant role. The extent of orbital overlap depends critically on both mutual orientation and spacing within the encounter complex. Our MD simulations suggest that complexation of a cation forces the quinoid walls of the calix[4]arene into a cone conformation where, because of stereological factors, they are unable to adopt a cofacial arrangement with the bpy's of the appended $[Ru(bpy)_3]^{2+}$ fragment. Electrostatic repulsion between the two cations pushes the luminophore away from the receptor, and we have found that the degree of emission quenching shows a clear correlation with the charge of the incoming cation. Thus, the characteristic triplet lifetime of the complex reflects the overall charge resident on the molecule but does not recognize the nature of the bound cation. An additional electrostatic effect is apparent from the binding constants measured for different cations where, in general, dications are bound more weakly than monocations but more strongly than trications. In fact, replacing the dicationic luminophore **Ru(Q)** with a neutral analogue[71] gives a 180-fold increase in the stability constant of the barium complex but eliminates the enhancement of luminescence that characterizes cation complexation to **Ru(Q)**.

Acknowledgment. We thank Johnson-Matthey PLC for their generous loan of precious metal salts. Financial support from the Royal Society of London, the CNRS, the Université Louis Pasteur, and ECPM is gratefully acknowledged. G.W. also acknowledges the CNRS IDQIS for allocation of computer resources.

Supporting Information Available: Table S1 of average angles and fluctuations of the **Ru**(**Q**) and **Ru_2**(**Q**) ligands and their barium complexes, Figure S1 giving the atom types used in the AMBER calculations on the quinone, anisole, and Ru−bipyridine fragments of **Ru**(**Q**) and **Ru_2**(**Q**), Figure S2 giving the atomic charges on fragments of uncomplexed **Ru**(**Q**) and **Ru_2**(**Q**), Figure S3 giving atomic charges on fragments of $Ba(ClO_4)_2$ complexes of **Ru**(**Q**) and **Ru_2**(**Q**), and Figures S4 and S5 giving the time evolution of the shortest distances between H_{pyr} protons of $Ru(bpy)_3$ and O_Q quinolic oxygens and between the center of mass of bipyridines of $Ru(bpy)_3$ and the center of mass of quinolic carbonyles, respectively (6 pages, print/PDF). See any current masthead page for ordering information and Web access instructions.

JA982786V

(69) The nature of any other ligands bound to zinc(II) is unknown, and it is important to stress that trace amounts of water are present in the system since the salt is hydrated.

(70) McConnel, H. *J. Chem. Phys*. **1961**, *35*, 508.

(71) For this experiment, the $[Ru(bpy)_3]^{2+}$ fragment of **Ru(Q)** was replaced with the neutral unit $[Re(bpy)(CO)_3Cl]$, and it was found that complexation of barium perchlorate caused an increase in the rate of light-induced electron transfer. See ref 67 for details.